BACHELOR

On the (de) hydration of K2CO3 in vacuum conditions

Brinkman, L.M.

Award date:
2019

EINDHOVEN UNIVERSITY OF TECHNOLOGY

Department of Applied Physics
Transport in Permeable Media

On the (de)Hydration of K_2CO_3 in Vacuum Conditions

Bachelor Thesis

Luc Brinkman

Supervisors:
dr. ir. Henk Huinink
ir. Jelle Houben

Eindhoven, Thursday 16th May, 2019

Contents

Chapter 1

Introduction

1.1 Energy transition and Domestic Heating

In the ongoing energy transition, humanity is challenged to make all its processes sustainable. A large part of this challenge is to use only renewable energy sources. While the generation of renewable energy is making good progress, with prices of solar and wind energy dropping below prices of conventional energy, these sources do create a new challenge. Generation of wind and solar energy are intermittent, thus we rely on nature's randomness, and seasonal and daily cycles. A solution is to store renewable energy with a range of techniques varying in energetic efficiencies, time scales, prices, and scalability.
There is currently no universal renewable energy carrier. For example, whereas Lithium-ion batteries are conquering the personal transportation market, it is not convenient for seasonal energy storage because of high prices and relatively low scalability.
One market that currently has no fully developed sustainable solution is domestic heating. Current regimes are heating by natural gas (e.g. in The Netherlands), electric heating (e.g. in France), or the usage of solar boilers (e.g. in Turkey [1]). Whereas solar boilers are applicable in warm countries with much sun, they are less efficient in many colder countries. Further increasing the pressure to find a sustainable alternative to natural gas heating in The Netherlands, is the decision to gradually decrease gas extraction until it is ceased entirely by 2030. The decision was caused by years of earthquakes in Groningen caused by extraction of natural gas in that region.
Amongst potential renewable alternatives for domestic heating are geothermal heating, (domestic) heat pumps, industrial waste heat, electric heating (with renewable energy), sensible thermal energy storage in water or molten salt, and thermochemical energy storage in salt hydrates.
Salt hydrates are thermochemical materials that store and release energy by cyclically dehydrating and hydrating respectively. A literature study was performed by Donkers et al. [2], which has led to further research and a current focus on K_2CO_3 as a thermochemical material.

1.2 Thermochemical Energy Storage System

A system for thermochemical energy storage dehydrates a thermochemical material (TCM) such as K_2CO_3 to store energy, and hydrates it to release energy. A humidifier is used to provide and condense water vapor, and a heat exchanger supplies and extracts energy. Such a system could be installed at household scale and provide hot tap water and central heating on demand.

There are two general ways to configure such a reactor, called the 'closed system' and 'open system', schematically shown in Figure 1.2. An alteration of the latter called 'closed loop system' is also possible. The key properties of these reactor types are compared in Table 1.1, and are discussed below. An open reactor has one main compartment carrying the TCM. An external water source (e.g. tap water) is used for evaporating and condensing vapor. There is air and water vapor in the TCM compartment, which are circulated by forced convection. Locally, vapor transport may be diffusion dominated. A

closed reactor is closed from its surroundings and works under vacuum conditions. A water reservoir is included in the system, and is cooled/heated e.g. by another, external water source. Water vapor is the only present gas in the system, thus its transport is dominated by natural convection. In a simplistic view, a valve between the TCM compartment and the water reservoir can be operated to control the energy output of the system.
Besides the vapor transport, the heat transport also differs between closed and open systems. In a closed system there is barely any atmosphere to transport heat, so heat transport is dominated by conduction through the thermochemical material and any additional heat exchanger (e.g. metal fins) in the reactor. In an open system heat is transported by convection of the air and water vapor. Depending on reactor dimensions, an open system may have difficulty to reach a high temperature. If the heat capacity of the flowing gas is too big relative to the energy release of the K_2CO_3, the available heat is diluted to a temperature below the maximum hydration temperature. To tackle this limitation a closed loop system has been proposed. A closed loop system is comparable to an open system in its transport mechanisms, but works at a controlled variable air pressure to better regulate the output temperature.

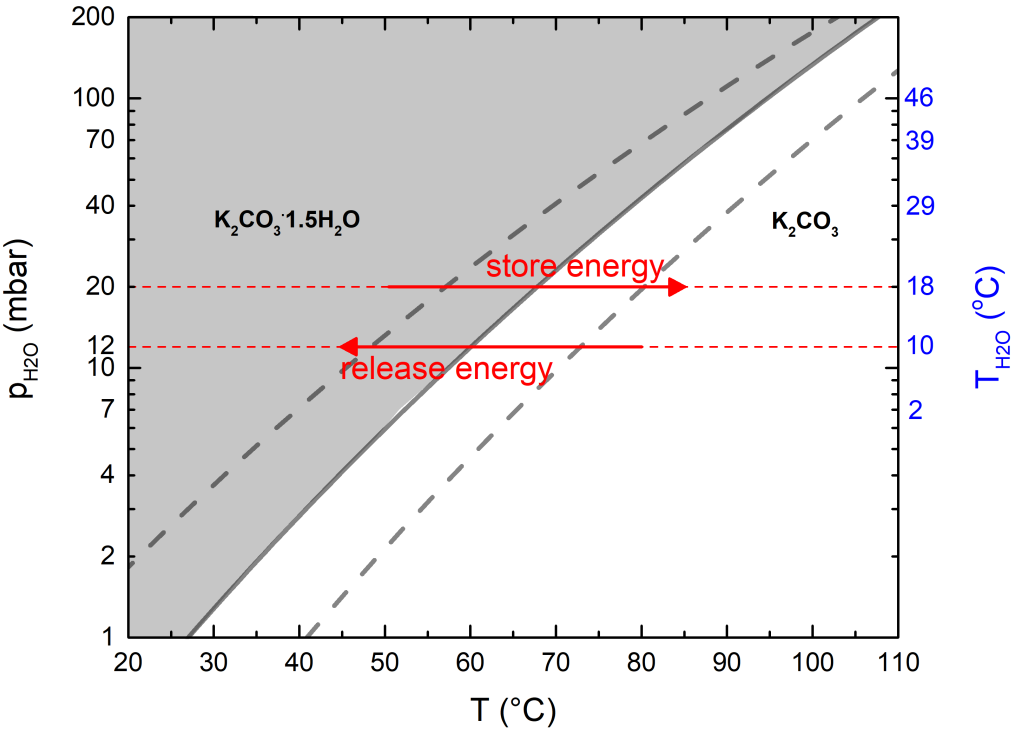

Figure 1.1: The phase-diagram of K_2CO_3, showing the water vapor pressure against the sample temperature. The right y-axis shows the corresponding water reservoir temperature. The red dashed lines show the expected working pressures for energy storage and release. In the white area the material dehydrates to the α phase and releases energy. In the gray area the material hydrates to β phase, which stores energy. At the gray line, the two phases are in equilibrium. The dashed gray lines show the metastable zone boundaries, in-between which reaction onset is delayed by an induction time.

The (de)hydration reaction of K_2CO_3 is denoted by:

$$\mathrm{K_2CO_3 \cdot 1.5H_2O(s) \rightleftharpoons K_2CO_3(s) + 1.5H_2O(g)}, \tag{1.1}$$

in which the dehydration reaction (left to right) is endothermic and the hydration reaction is exothermic. The cycle can be completed many times before the K_2CO_3 degrades[5]. For TCMs in general, the less hydrated phase is referred to as the α phase, and β is the hydrated phase.
The (de)hydration reaction of K_2CO_3 is governed by the temperature of the material and the surrounding water vapor pressure. The corresponding phase-diagram is shown in Figure 1.1. The gray line indicates the equilibrium water vapor pressure p_{eq} of K_2CO_3 as a function of temperature. At vapor pressures higher than the equilibrium vapor pressure (i.e. $p_{H_2O}/p_{eq} > 1$, marked gray) the material hydrates, whereas for lower vapor pressures ($p_{H_2O}/p_{eq} < 1$, marked white) the material dehydrates.
The temperature of (de)hydration depends on the available water vapor pressure, which in turn depends on the temperature of available water. In the winter typical water temperatures are $10\,^{\circ}\mathrm{C}$, so the corresponding $p_{H_2O} = 12\,\mathrm{mbar}$ should be used as the expected working pressure for energy release upon hydration. In the summer water is typically $18\,^{\circ}\mathrm{C}$, providing $p_{H_2O} = 20\,\mathrm{mbar}$, which is thus the expected working pressure for energy storage by dehydration. These expected pressures for storage and release are indicated by the red arrows in Figure 1.1.
The presence of a metastable region (the area between the dashed lines in Figure 1.1) limits both reaction onset and reaction rate. Metastability is the phenomenon where net energy can be gained by a phase change only after overcoming an energy barrier which hinders the phase change from starting. This is explained in detail in section 2.1. The vapor pressure for which reactions onset is called the critical pressure p^* and corresponds to the dashed line, also called the "metastable zone boundary". For example, when cooling a fully dehydrated sample, hydration does not start upon reaching (p_{eq}, T) but at (p^*, T). Within the metastable zone bulk (de)hydration starts only after an induction time τ. The (de)hydration behavior of K_2CO_3 is well described by classical nucleation theory, which is explained in section 2.1.

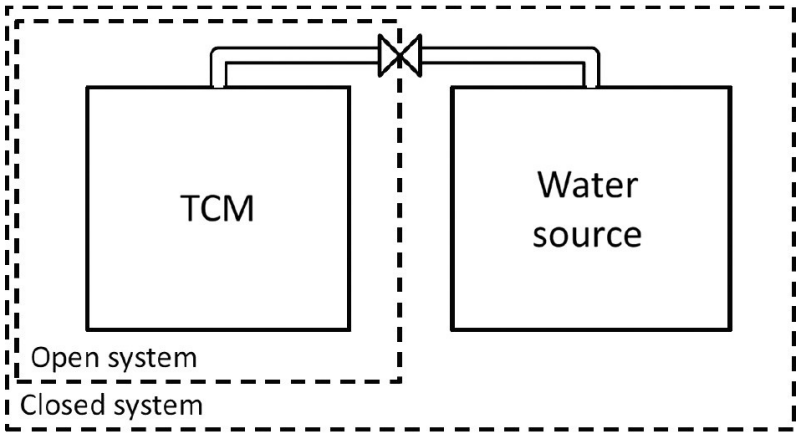

Figure 1.2: Schematic depiction of open and closed systems for thermochemical energy storage. An open system consists of a TCM compartment and uses an external water source for evaporation/condensation. A closed system includes a water source, which is cooled and heated by an external (water) source. Source: [6]

Table 1.1: A comparison of some important properties for different reactor types.

	Closed System	Open System	Closed Loop System
Atmosphere	Vacuum	1 atm	0-3 atm
Vapor Transport	Natural convection	Forced convection	Forced convection
Heat Transport	Conduction	Convection	Convection

The (de)hydration behavior of K_2CO_3 in atmosphere (resembling an open system) has been studied extensively [5, 6], while little research has been done in vacuum conditions. The thermodynamics (i.e. the phase line $p_{eq}(T)$) are the same regardless the presence of inert gases (air), and are thus independent on reactor type. The kinetics could differ between vacuum and atmospheric conditions. This thesis tries to answer how the metastable zone, induction time, and corresponding surface energy of K_2CO_3 in vacuum conditions compare to those in atmosphere. It will then try to conclude which reaction mechanism is responsible for hydration in vacuum, and compare it to present literature for atmospheric conditions.

Comparison of Vacuum and Atmospheric Conditions

The kinetics of K_2CO_3 hydration depend, amongst other things, on the water vapor transport to the K_2CO_3 surface and into the material. For hydration nucleation to occur, enough water molecules should meet at the K_2CO_3 surface whilst enough energy is locally available to start a reaction. To perceive the stochastic nature of this process, it is useful to evaluate a $10 \times 10 \times 10\,\mathrm{nm} = 10^{-24}\,\mathrm{m}^3$ cube in typical hydration conditions: $p_{H_2O} = 12\,\mathrm{mbar} = 12 \cdot 10^2\,\mathrm{pa}$ at $50\,^\circ\mathrm{C} = 323.15\,\mathrm{K}$. The ideal gas law $pV = Nk_BT$ gives

$$12 \cdot 10^2 \cdot 10^{-24} = N 1.38 \cdot 10^{-23} \cdot 323.15 \Rightarrow N = \frac{120}{1.38 \cdot 323.15} = 0.269 \tag{1.2}$$

water molecules in the cube, which is not many. In case of a closed system the water vapor is the only present gas. In case of an open system there is $1\,\mathrm{atm}$ of air present besides the water. This means that in an open system the cube holds approximately 22 gas molecules, of which less than one is water. This might have an effect on the kinetics. With this in mind, it is useful to examine a real life closed system. Ideally, the system would operate under vacuum conditions with only water vapor present. However, a system might have residual air molecules, or a small leakage causing the presence of air in the system to grow. To illustrate the effects of a small presence of air molecules, here is an example: *there is $12\,mbar$ of water vapor and $5\,mbar$ of air (due to a leakage). Initially, both gases are evenly dispersed. When the TCM is hydrating, there is a flow from the water reservoir to the TCM, due to natural convection. New water vapor is evaporated at the reservoir, and water vapor is absorbed at the TCM. The air is inert and does not condense, and it moves towards the TCM in the convective flow. Hence, the air will concentrate near the TCM and form a non-condensible layer. In this region the non-condensible layer effectively blocks the convection term of (vapor) transport, so the vapor transport locally becomes diffusion dominated.* Because the diffusion term is much smaller than the convection term (without a non-condensible layer), this mechanism might limit hydration kinetics, even with only a small presence of air molecules in a closed system.

Hydration pathways

Based on present literature, there are two main pathways in which hydration can occur: 1.) a direct solid-solid transition; 2.) a pathway consisting of two steps, where first the α state dissolves and the liquid recrystallizes into the β state. These pathways are depicted in Figure 1.3.
A recent study by Sögütoglu et al. demonstrates that the K_2CO_3 hydration reaction follow the solid-solid pathway, while the reaction is mediated by a local wetting layer between the α cluster and the bulk β[6]. The idea is that a true solid-solid transition is unlikely because some mobility is required at the boundary between the two phases. A wetting layer is a local dissolution that creates the mobility needed for changing the crystal structure from α to β phase. This is schematically depicted in Figure 1.4. This interface is expected to become thicker and more mobile at higher supersaturations (or, approaching the deliquescence pressure of phase α.
Sögütoglu's conclusion that a wetting layer mediates the hydration reaction was supported by a matching interfacial energy γ, which was calculated by measuring the induction time τ for different supersaturations.

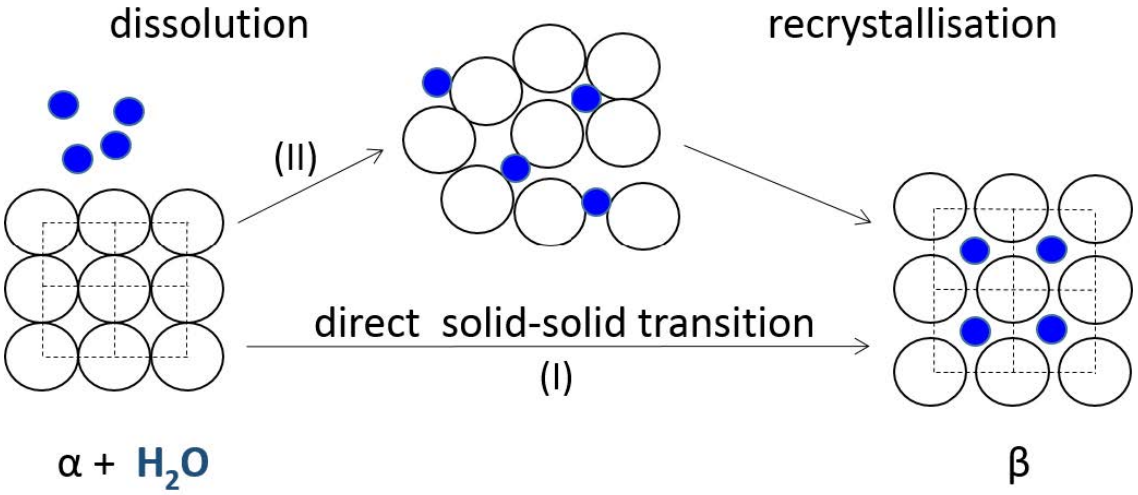

Figure 1.3: Two hydration pathways[6]. ToDo: expand this caption

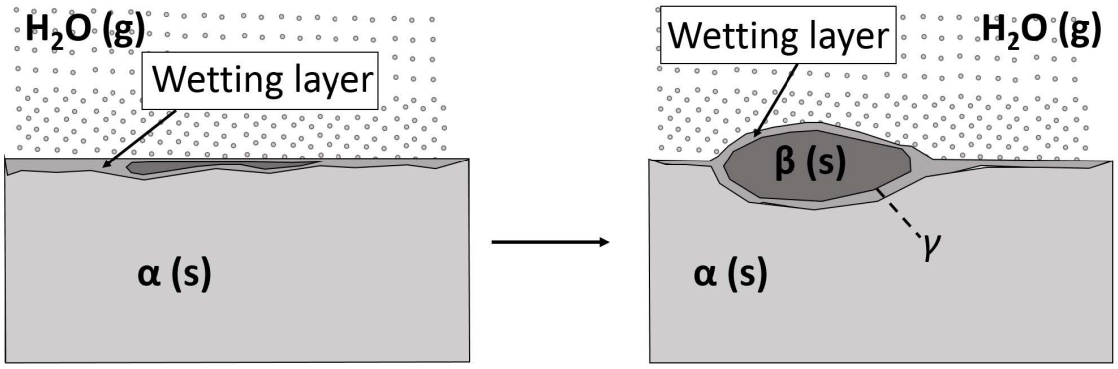

Figure 1.4: Schematic overview of the phase change from α to β phase. The phase change can be considered as a solid-solid transition mobilized by a wetting layer.

1.3 Aim and Approach

This thesis looks into some of the properties of (de)hydration of K_2CO_3 in vacuum conditions with the goal of better understanding the phase change, to eventually progress the developments of thermochemical materials as an energy carrier for domestic heating.
To study the metastable zone boundary, onset temperatures are measured at different pressures and are compared to previous atmospheric results by Sögütoglu[5, 6].
To study the hydration mechanism in vacuum conditions, the conduction time τ is measured from which the interfacial energy γ is calculated. These results are again compared to Sögütoglu's atmospheric results and the hydration mechanism for vacuum conditions is concluded.

Chapter 2

Theory

2.1 Classical Nucleation Theory

The nucleation behavior and the presence of a metastable zone for K_2CO_3 are well described by classical homogeneous nucleation theory (CNT). Nucleation theory describes how a phase (β) can grow in a bulk phase (α) through the formation and growth of nuclei. The following theory explains the basics of CNT and then summarizes the most important aspects as needed for understanding the hydration behavior of K_2CO_3. The chapter is adapted from the book *Nucleation Theory* by V.I. Kalikmanov [4] and from Sögütoglu (2019)[6].

A metastable state corresponds to a local minimum of free energy for the p, T conditions. The global minimum free energy, corresponding to the equilibrium state, can be achieved by overcoming an energy barrier. This is shown in Figure 2.1a.

For hydrating K_2CO_3 this means the following: In the white area in Figure 1.1, a dehydrated sample is stable. In the gray area within the metastable zone, the dehydrated sample is metastable. It will proceed to its (stable) hydrated state only after overcoming an energy barrier. In the gray area outside the metastable zone, the sample will immediately start hydrating without the need of overcoming an energy barrier. For K_2CO_3, the hydration and dehydration mechanisms are not necessarily the same. This thesis focuses mainly on the hydration of K_2CO_3, so the following theory is explained for the hydration phase change only.

A phase change starts with the formation of a small cluster, or nucleus, which can then grow or shrink. The Gibbs free energy of such a cluster is

$$\Delta G = -\frac{V}{\nu}(b-a)\Delta\mu + \gamma A, \tag{2.1}$$

where $V\,[\mathrm{m}^3]$ is the volume of the cluster, $v\,[\mathrm{m}^3]$ is the volume of one $\mathrm{K_2CO_3 \cdot 1.5H_2O(s)}$ unit, b and a are the amount of water molecules in one hydrated and dehydrated salt unit respectively ($a = 0$ and $b = 1.5$ for K_2CO_3),

$$\Delta\mu = k_B T \ln(p/p_{eq}) \tag{2.2}$$

is the chemical potential, γ is the interfacial surface energy and A is the surface area of the cluster. Both the volume V and area A are functions of cluster size r, so $\Delta G = \Delta G(r)$ and it is shown in Figure 2.1b. The supersaturation p/p_{eq} is the driving force of the hydration.

The energy barrier that must be overcome corresponds to the maximum of $\Delta G(r)$, so it can be found using

$$\left(\frac{\partial \Delta G(r)}{\partial r}\right)_T = 0. \tag{2.3}$$

The energy barrier is denoted as

$$\Delta G^* = \Delta G(r^*), \tag{2.4}$$

where r^* is the critical cluster size. On average, clusters larger than r^* will grow and smaller clusters will dissociate (shrink). Because of energy fluctuations ($\mathcal{O}(k_B T)$) the process is stochastic, so it is

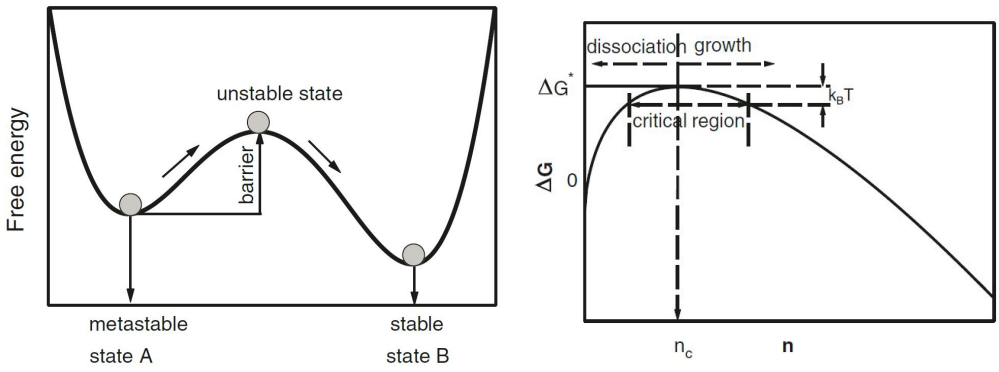

(a) Free energy.

(b) Energy barrier: Gibbs free energy.

Figure 2.1: Two representations of the energy barrier. Source: [4]

better to speak of a critical region than of a critical size. Clusters larger than the upper limit of the critical region will inevitably grow.

The volume V and surface area A depend on mechanism of cluster growth. There are two main mechanisms for a cluster to grow:
1: The 1.5-hydrate salt cluster (β) grows as a disc on the surface of the 0-hydrate salt (α), where it grows in 2D to the sides, layer by layer.
2: The β cluster grows overlayer mode, which is the case for a uniform expansion of the nucleus. Such a 3D shape can be spherical or hemispherical.
These cluster shapes are shown schematically in Figure 2.2. Using the volumes and surface areas for a disc, sphere, and hemisphere and solving Equation 2.3 finally yields

$$r^*_{2D} = \frac{v\gamma}{(b-a)k_B T \ln(p/p_{eq})} \tag{2.5}$$

$$r^*_{3D} = \frac{2v\gamma}{(b-a)k_B T \ln(p/p_{eq})} = 2r^*_{2D} \tag{2.6}$$

and

$$\Delta G^*_{2D} = \frac{h\pi v\gamma^2}{(b-a)k_B T \ln(p/p_{eq})} \tag{2.7}$$

$$\Delta G^*_{3D} = \frac{\eta\pi v^2\gamma^3}{(b-a)^2 k_B T \ln^2(p/p_{eq})}. \tag{2.8}$$

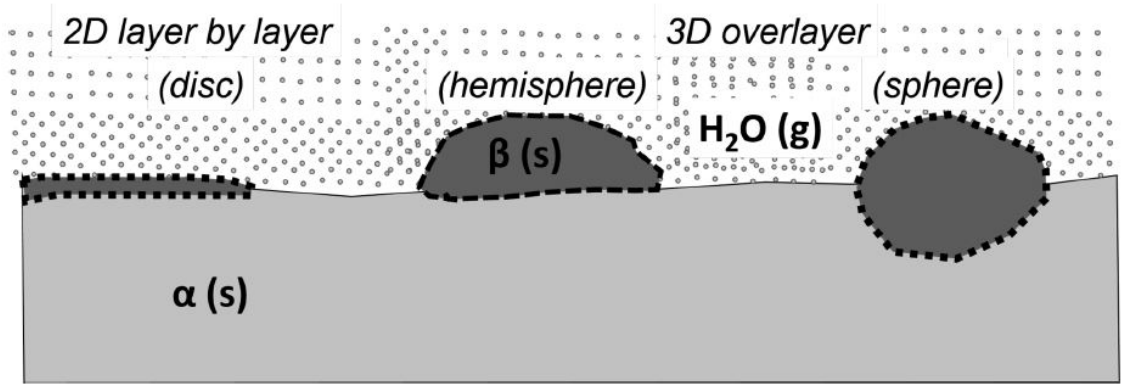

Figure 2.2: Schematic overview of the ways in which a cluster can grow[6].

2.2 Interfacial Energy

We are interested in the interfacial surface energy γ This energy can be calculated by measuring the induction times for different temperatures and supersaturations. The induction time is given by

$$\tau \equiv \frac{c}{J}, \tag{2.9}$$

where c is a proportionality constant and J is the nucleation rate. The nucleation rate is defined as the number of nuclei (of any size) that are formed per unite time, and it is given by

$$J = \kappa \exp\left(\frac{-\Delta G^*}{k_B T}\right) = N_s j \mathcal{Z} \exp\left(\frac{-\Delta G^*}{k_B T}\right), \tag{2.10}$$

where N_s is the number of nucleation sites, j is the rate at which molecules attach to the cluster (causing it to grow), and $\mathcal{Z}$ is the Zeldovich factor. The Zeldovich factor is inversely proportional to the with of the critical region the critical region, and can be interpreted as the probability that a nucleus grows to form the new phase (as opposed to it dissolves). Substituting Equation 2.9 gives

$$c/\tau = \kappa \exp\left(\frac{-\Delta G^*}{k_B T}\right) \Rightarrow \ln(\tau^{-1}) = \ln\frac{\kappa}{c} - \frac{\Delta G^*}{k_B T} \tag{2.11}$$

and substituting Equation 2.7 and Equation 2.8 gives

$$\ln(\tau^{-1}) = \ln\frac{\kappa}{c} - \lambda \cdot \frac{1}{\ln^n(p/p_{eq})}, \tag{2.12}$$

with $n = 1$ for 2D nucleation and $n = 2$ for 3D nucleation, where

$$\lambda_{2D} = \frac{h\pi v \gamma^2}{(k_B T)^2 (b - a)} \tag{2.13}$$

and

$$\lambda_{3D} = \frac{\eta\pi v^2 \gamma^3}{(k_B T)^3 (b - a)^2}. \tag{2.14}$$

Filling in a=0, b=1.5 for K_2CO_3 and solving for γ we get

$$\gamma_{2D} = \left(\frac{1.5(k_B T)^2 \lambda_{2D}}{h\pi v}\right)^{1/2} = k_B T \left(\frac{1.5\lambda_{2D}}{h\pi v}\right)^{1/2} \tag{2.15}$$

and

$$\gamma_{3D} = \left(\frac{1.5^2 (k_B T)^3 \lambda_{3D}}{h\pi v^2}\right)^{1/3} = k_B T \left(\frac{1.5^2 \lambda_{3D}}{\eta\pi v^2}\right)^{1/3}. \tag{2.16}$$

Equation 2.12 is used as a fit function on induction time measurements in which λ is the slope, so λ can be determined from the measurements. For K_2CO_3 $v = 124.0 \cdot 10^{-30}\,\mathrm{m}^3$ and $h = 7.1093 \cdot 10^{-10}\,\mathrm{m}$. From this the interfacial surface energy γ can be calculated.

Chapter 3

Setup and Methods

Two categories of experiments are performed to study the de(hydration) of K_2CO_3 in vacuum, corresponding to a closed reactor. Firstly, the metastable zone boundary is investigated by measuring the onset temperatures at different pressures. Secondly, induction times are measured for different supersaturations within the metastable zone. Both types of experiments are performed with a single setup, which was previously constructed in a Master graduation project. The experimental setup and the improvements made to it, calibrations, and the methods used for the different measurements, are elaborated upon in this chapter.

3.1 Experimental Setup

The experiments generally involve measuring the mass of a sample of K_2CO_3 in response to different temperatures ($T_{K_2CO_3}$) and water vapor pressures (p_{H_2O}) under vacuum conditions. Thereby the experiments have a lot in common with Thermal Gravimetric Analysis (TGA), with the addition of vacuum and controllable water vapor pressure.
A schematic drawing of the setup is shown in Figure 3.1. The setup consists of two main chambers. One acts as a water reservoir with temperature T_{H_2O} that can be set with a (PID-controlled) heater to control p_{H_2O} (equilibrium water vapor pressure is a function of water temperature). The other chamber is denoted 'sample holder'. A copper container is placed in the sample holder and is filled with K_2CO_3 grains. The function of the copper container is to distribute heat throughout the K_2CO_3 sample so its temperature $T_{K_2CO_3}$ is more homogeneous. The sample holder is heated by a second heating element to control $T_{K_2CO}3$. The sample temperature and the function of the copper container are further discussed in section 3.4. The sample holder is carried by a frame that is placed on a mass balance, so the mass of the sample can be measured as a function of time.
The water reservoir is connected to a pressure sensor via stainless steel tubing and to the sample holder via a flexible hose. The flexible hose mechanically decouples the sample holder from the rest of the setup and allows the sample's mass to measured. A vacuum pump is connected via a valve, which is closed during experiments. There is also an electronic valve in-between the water reservoir and the sample. This valve can be opened and closed during experiments. Because the system is in vacuum (i.e. $p = p_{H_2O}$) the transport of water vapor is convection dominated. Therefore, p_{H_2O} can be assumed homogeneous throughout the system.
Two thermocouples are placed inside the copper container, which is then filled with K_2CO_3 grains. One thermocouple is attached to the copper wall of the container, the other is positioned in the bulk of K_2CO_3. Together these thermocouples span the temperature range of the sample. This is further explained in section 3.4.

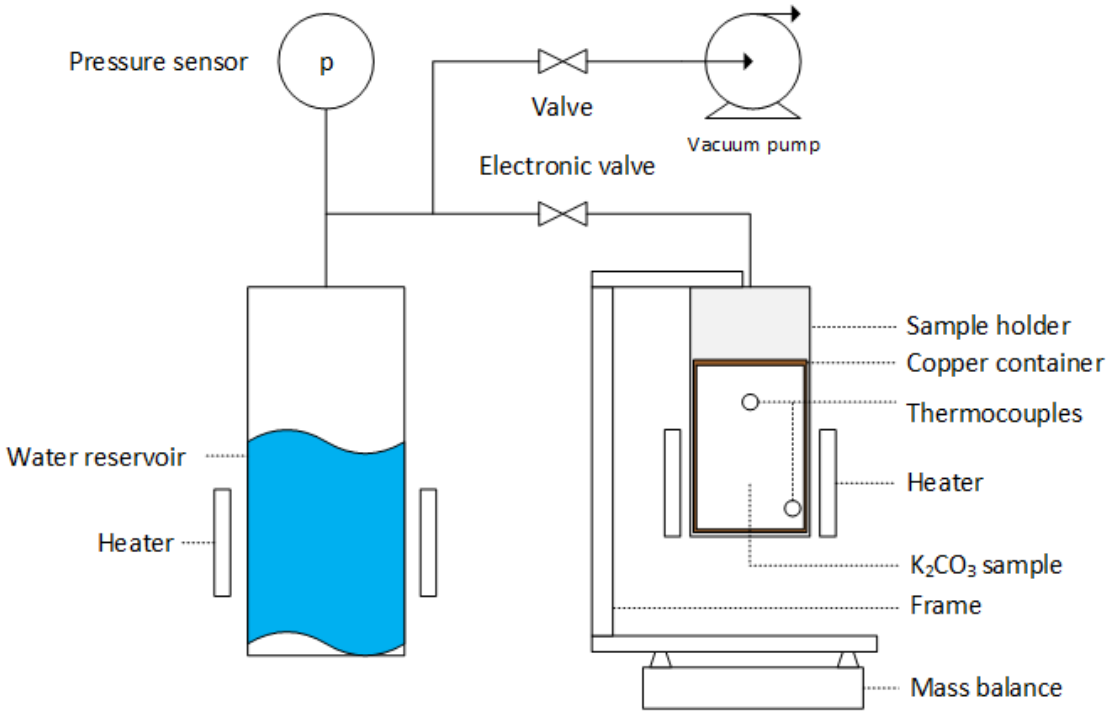

Figure 3.1: Schematic drawing of the experimental setup. A heated water reservoir is used to provide a water vapor pressure. A K_2CO_3 sample is placed in a container and is also heated. The mass response of the K_2CO_3 to different pressures and temperatures is measured by a mass balance.

3.2 Mass balance

In the experiments the mass is measured to determine the kinetics of K_2CO_3 (de)hydration. In early testing irregularities in the measured mass were observed. A nearly 70 hour experiment to calibrate the mass balance is shown in Figure 3.2. In this experiment the entire setup is connected in the same way as during experiments, the sample holder is empty. The temperature of the sample holder is alternated between 30 and $100\,^{\circ}\mathrm{C}$. Not all the mass of the sample holder weighs on the mass balance, because it is also connected by a flexible hose to another frame on the side of the water reservoir. This means that, potentially, an increase of mass in the sample holder would only be measured partially by the mass balance, whilst part of the added weight is diverted by the hose to the frame of the water reservoir. When parts of the setup move, the relative weight diversion by the hose can also change, leading to further deviations. The latter mainly occurs due to changes in temperature. Roughly speaking, two kinds of mass fluctuations can be identified:

- random mass fluctuations / drift;
- temperature effects on measured mass.

The random mass drift, with a characteristic time of hours, is possibly caused by relaxation of the system, with changing tensions causing more weight to be diverted away from the mass balance to the frame - or vice versa. Fluctuations, with a characteristic time of seconds to minutes, are in the order of $10\,\mathrm{mg}$ and could be caused by air flows in the room, vibrations caused by the LAUDA, and the mass balance not being designed for long continuous measurements. These effects are mitigated by using a partial wind shield around the setup and using a flexible hose to connect the frame and the sample holder. Compared to the mass changes in the experiments with K_2CO_3, the measured fluctuations are small enough and the drift is slow enough in order not to have a significant impact on the experiments. The mass changes caused by temperature changes, however, are larger and can lead to confusion about

phase change onset temperature and uncertainty in reaction rate. Therefore it is preferred to mitigate this effect, which is described in section 3.3.

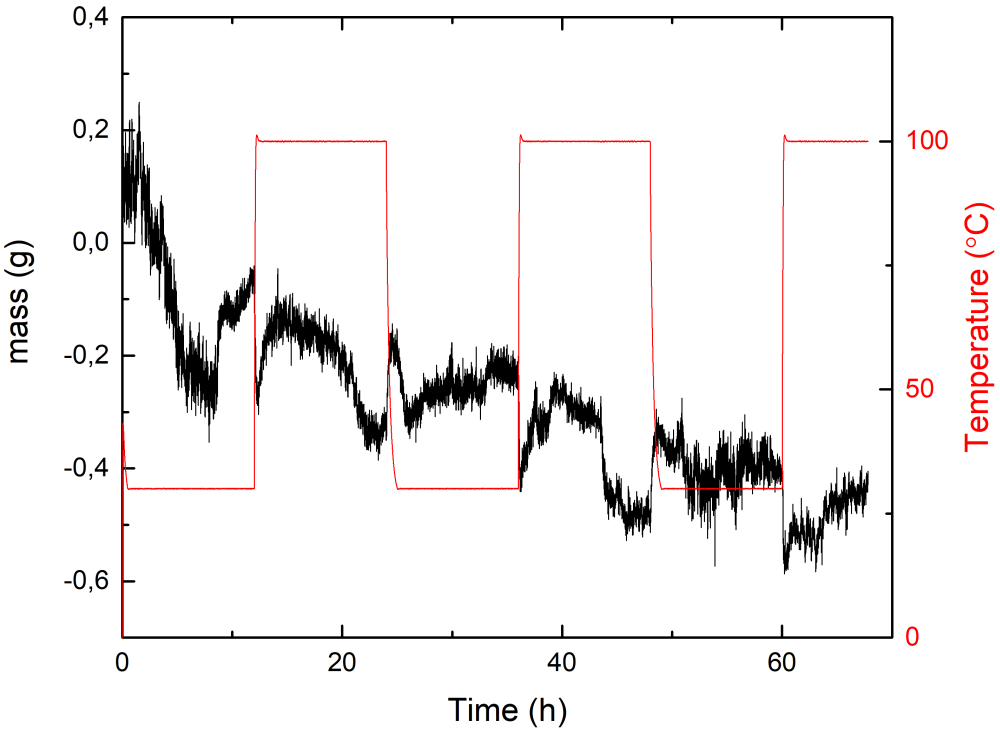

Figure 3.2: Calibration measurement to find the mass fluctuations with alternating temperatures. The sample holder is empty, so no chemical reactions can occur. The left y-axis shows the measured mass and the right y-axis shows the imposed temperature.

3.3 Temperature Effects on Measured Mass

In early experiments, it was observed that the measured mass reacted to the temperature of the setup. At first we thought the mass balance (which works magnetically) was affected by the electromagnetic field caused by the heater. MuMetal shielding and increasing the distance between the balance and the heater were tested, but did not remove the problem. A further test with the heater slightly above the mass balance, but mechanically decoupled (i.e. it was hanging from a frame disconnected from the balance), showed zero correlation between measured mass and heater power.

The next hypothesis was that the heating of the setup influenced the mechanical properties of the system, causing the amount of weight diverted to the frame to change. This might be caused by thermal expansion of some parts, causing the shape of the setup to change slightly.
The link between temperature and mass was confirmed by a simple experiment where the majority of the setup is $60\,^{\circ}\mathrm{C}$ whereas the sample holder (holding no K_2CO_3) was heated from room temperature to $60\,^{\circ}\mathrm{C}$, causing a large mass increase of $12\,\mathrm{g}$. This mass change was much larger than observed in previous experiments. This experiment was performed with the setup as a closed system with nor-

mal atmosphere inside. Quantitatively determining the effect of different possible improvements was difficult, because the experiments were not very reproducible. Patterns did repeat, but amplitudes change between periods and mainly between experiments. There had even been instances where the mass increased with temperature (as opposed to decreased). A final experiment, trying to reproduce previous, more favorable, mass responses was performed in vacuum. The observed mass changes were about one order of magnitude smaller than with the exact same setup in atmospheric pressure.

This has led to the final realization that the temperature of the sample holder influences the temperature of the gas inside the setup, and thus the pressure. The changing pressure moves the flexible hose, altering its mechanical properties, thus changing the weight on the balance. This effect is larger for greater pressures. It has also been minimized by trying out slightly different the positions of the sample holder, and settling for a position and attachment method that are reproducible and have minimal temperature influences on the weighed mass.

3.4 Sample Temperature

In early tests the K_2CO_3 grains were placed directly in the sample holder, as sketched in Figure 3.3a. Large inhomogeneities in the sample temperature were observed. The maximum temperature difference that occurs within the sample during an experiment at a certain heating/cooling rate, ΔT_{exp}, of up to $15\,\mathrm{K}$ was observed during heating. The experiments of this work benefit from a homogeneous temperature within the sample. This has been the reason for COMSOL simulations and subsequent improvement of the setup, with the goal of limiting ΔT_{exp} to $1\,\mathrm{K}$. Analogous to ΔT_{exp}, ΔT_{sim} is defined as the maximum temperature difference within the sample during a *simulated* experiment. The goal of the COMSOL simulations was to find possible changes to the setup to decrease ΔT_{sim} to $1\,\mathrm{K}$. Subsequently the changes were applied and the resulting ΔT_{exp} was measured during experiments. The final results is an improved setup with ΔT_{exp} reduced to $2\,\mathrm{K}$ for heating/cooling rates of up to $1\,\mathrm{K/min}$. While this exceeds the original goal, it allows for measurements with an acceptable uncertainty. This section has the structure of a separate report within the thesis. It starts with describing the method, followed by the results of the simulations and the experiments performed on the improved design. It then ends with a small conclusion.

3.4.1 Method

In COMSOL Multiphysics the existing setup is sketched using known material properties of steel and K_2CO_3 grains. The "Heat transfer in Solids (ht)" toolkit is used to simulate the thermodynamics. ΔT_{exp} is defined as the experimentally measured temperature difference between the inner and outer thermocouples in the sample. It is known that $\Delta T_{exp} = 15 - 17\,^{\circ}\mathrm{C}$ at a heating rate of approximately $10\,\mathrm{K/min}$ at the heater and $4\,\mathrm{K/min}$ in the sample. The thermal conductivity $k\,[\mathrm{W/mK}]$ of a K_2CO_3 pill (compressed powder) is $k \approx 0.3\mathrm{W/mK}$[3]. The thermal conductivity of K_2CO_3 grains is not exactly known, so it can be used as an optimization parameter. The value of k of the K_2CO_3 is iterated until $\Delta T_{sim} = \Delta T_{exp}$, with ΔT_{sim} the simulated value of the temperature difference between (the positions of) the inner and outer thermocouples in the sample. Therefor, ΔT_{sim} is assessed at different times in the heating process and the maximum value is used. Once k is found such that $\Delta T_{sim} = \Delta T_{exp}$, the model is assumed to be correct. It can then be used to simulate new potential designs. Multiple new setups are designed and their ΔT simulated. A design that is both constructible and has a $\Delta T < 1\,\mathrm{K}$ is finally built and tested to verify whether the intended result has been reached (i.e. that $\Delta T_{exp} < 1\,\mathrm{K}$).

3.4.2 Results

Step 1: Optimizing for k

A sketch of the sample holder filled with K_2CO_3, as in the existing setup, is shown in Figure 3.3a. The sample holder consists of $2\,\mathrm{mm}$ steel and has a $10\,\mathrm{mm}$ thick bottom. It is filled with K_2CO_3 grains,

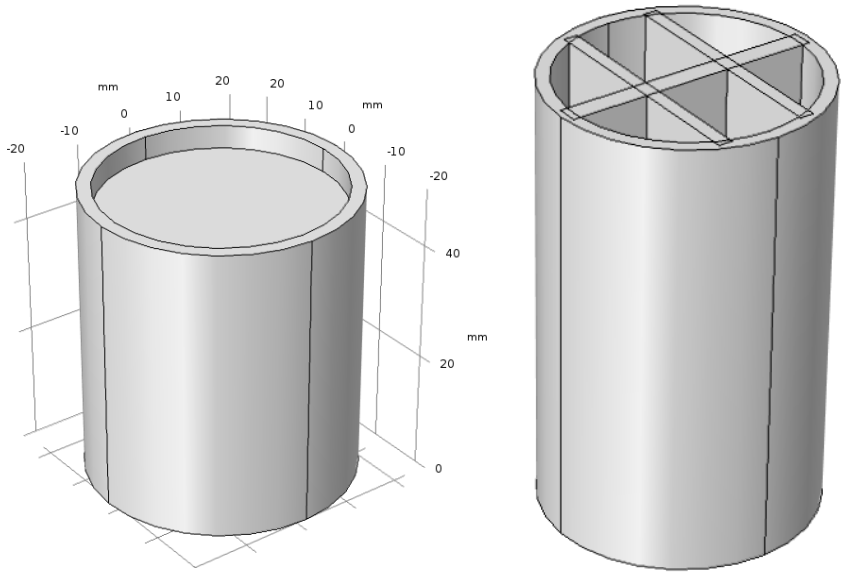

(a) The old setup: A sample holder filled with K_2CO_3.

(b) The designed copper container, which can be filled with K_2CO_3 and placed inside the sample holder.

Figure 3.3: Sketches in COMSOL Multiphysics.

Table 3.1: ΔT_{sim} at $t = 700\,\mathrm{s}$ for different values of k.

$k\,[\mathrm{W/mK}]$	$\Delta T_{sim}\,[\mathrm{K}]$ at $t = 700\,\mathrm{s}$
0.15	27
0.30	20
0.35	17
0.40	15
0.45	14

which are simulated as a bulk material. The outside surface of the container is heated, so it is considered to have a time-dependent temperature boundary condition, that increases linearly from 20 to $100\,^{\circ}\mathrm{C}$ at a rate of $6\,\mathrm{K/min}$.
Simulating the thermal response of the system to this boundary condition, it is found that the highest ΔT_{sim} occurs at $t = 700\,\mathrm{s}$. ΔT_{sim} for different values of k, at $t = 700\,\mathrm{s}$, is shown in Table 3.1. The optimized value of k is the range $0.35 - 0.40\,\mathrm{W/mK}$ (i.e. then $\Delta T_{sim} = \Delta T_{exp} = 15 - 17\,\mathrm{K}$). For the simulations with the new container designs $k = 0.35\,\mathrm{W/mK}$ is used. As a worst-case scenario, additional simulations with $k = 0.25\,\mathrm{W/mK}$ are performed.

Step 2: Simulations with New Container Designs

After some design iterations, a copper container with fins as shown in Figure 3.3b is chosen. The container can be filled with approximately $50\,\mathrm{g}$ K_2CO_3 and then be placed in the sample holder. The fins transport heat through the sample and thus cause a more homogeneous temperature. The bottom of the container is in thermal contact with the bottom of the sample holder. The outer diameter of the container is slightly smaller than the inner diameter of the sample holder, thus the sides of the two are not per se in thermal contact. It is plausible, however, that they make (thermal) contact along some edge. Therefore a contact between the sample holder and the container, $1\,\mathrm{mm}$ broad and over the

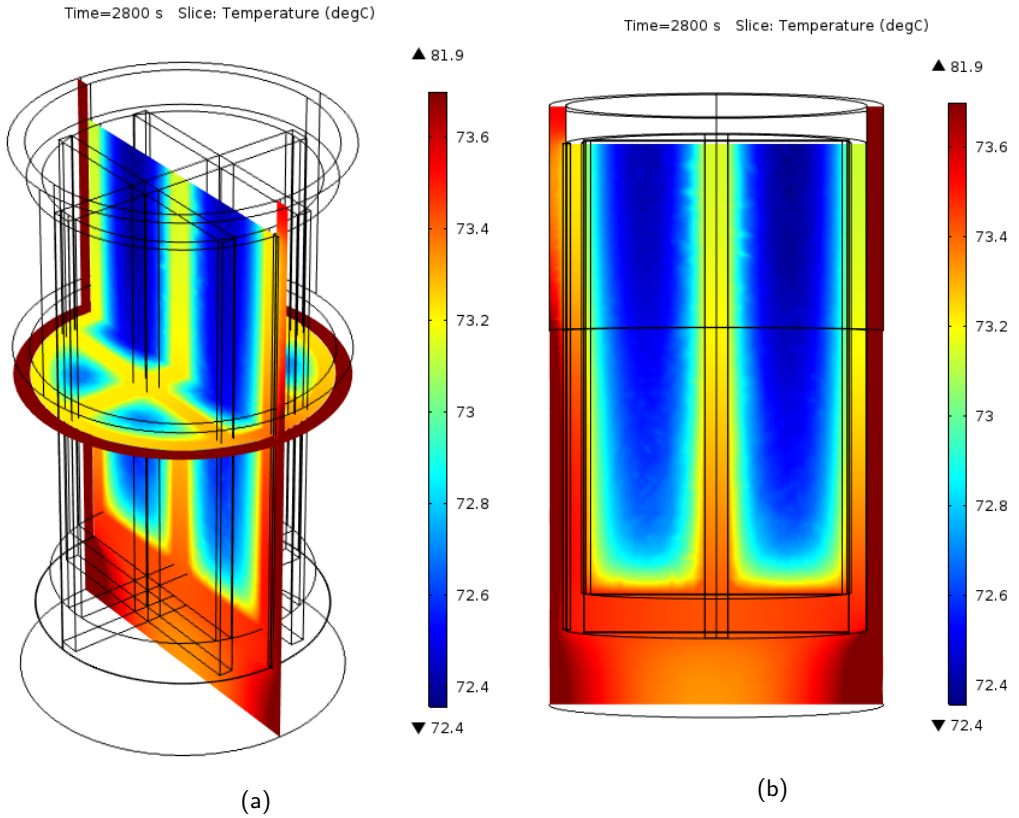

Figure 3.4: Simulated temperature profiles with a designed copper container with fins. The container is filled with K_2CO_3 and placed in the sample holder. A homogeneous boundary heat source heats the system from $20\,^{\circ}\mathrm{C}$. The shown profiles are at $t = 2800\,\mathrm{s}$.

entire height, is added to the simulation. The temperature boundary condition is replaced by a $50\,\mathrm{mm}$ high homogeneous boundary heat source to better simulate the heater. The chosen heating power is $6\,\mathrm{W}$, corresponding to a temperature rise of approximately $1\,\mathrm{K/min}$ – which is representative for the experiments.
The results are shown in Figure 3.4 for $k = 0.25\,\mathrm{W/mK}$ and $t = 2800\,\mathrm{s}$, the time with the highest ΔT_{sim}. From these simulations it is concluded that most heat is conducted through the bottom. The influence of the thermal contact edge can also be seen: in Figure 3.4b the left edge of the container is in thermal contact with the sample holder whereas the right edge is not. Heat is conducted through the left edge, resulting in a slightly higher temperature in the left half of the sample. ΔT_{sim} for multiple heating powers and k are shown in Table 3.2. For a heating rate of $1\,\mathrm{K/min}$ both $k = 0.35\,\mathrm{W/mK}$ and the worst-case scenario $k = 0.25\,\mathrm{W/mK}$ satisfy the $\Delta T \leq 1\,\mathrm{K}$ goal. For some experiments, a higher heating rate might be preferable. For $2\,\mathrm{K/min}$, ΔT_{sim} can be as high as $2\,\mathrm{K}$. This exceeds the $1\,\mathrm{K}$ goal, but is still much lower than the previously measured $17\,\mathrm{K}$ upon quick heating.
It should be noted that cooling is thermodynamically analogue to heating, thus the same ΔT's can be used. Because the setup is only passively cooled by convection of ambient air, the cooling rate is limited to approximately $1\,\mathrm{K/min}$, thus $\Delta T_{sim} \leq 1\,\mathrm{K}$ is always met.

Step 3: Measurements with New Container

After the simulations the copper container is manufactured and it is shown in Figure 3.5. This copper container can be filled with K_2CO_3 and placed into the sample holder. Two thermocouples are installed in the container. One is attached to the copper wall near the bottom, a place which the simulations

Table 3.2: ΔT_{sim} for different heat source powers and values of k.

Power [W] (Temperature gain [K/min])	k [W/mK]	$\Delta T_{sim,max}$ [K]
6 (1)	0.35	0.8
6 (1)	0.25	1.0
12 (2)	0.35	1.6
12 (2)	0.25	2.0

show is quick to respond to temperature changes of the heater. Its measured temperature is denoted T_{copper}. The other, denoted $T_{K_2CO_3}$, is placed approximately $1\,\mathrm{cm}$ from the top, in the bulk of the sample (away from any copper walls). Simulations show this position is slow to respond to temperature changes of the heater. Together these two thermocouples are thus likely to measure both the lowest and highest temperatures in the sample, so ΔT_{exp} can be found.
The improved system is tested by heating and cooling it at different rates, while vacuum conditions without water vapor make sure there are no hydration reactions. The results are shown in Figure 3.6. When using a step function for $T_{setpoint}$, the system heats up more quickly than it cools down, as heating is done electrically whereas cooling happens only by natural convection of the surrounding air. Cooling for high temperatures is quicker than cooling for lower temperatures because of the bigger temperature difference between the system and the ambient air. In the right half of the figure, the heating/cooling rate of the heater is set to $\pm 1\,\mathrm{K/min}$. For cooling with temperatures above $\approx 60\,^{\circ}\mathrm{C}$, both T_{copper} and $T_{K_2CO_3}$ follow this rate reasonably well, whereas for lower temperatures a cooling rate of $-1\,\mathrm{K/min}$ cannot be achieved. For heating, the sample nicely follows the heater with a rate of $+1\,\mathrm{K/min}$.
Figure 3.6 also shows ΔT_{exp}. For a heating/cooling rate of $\pm 1\,\mathrm{K/min}$, maximum ΔT is around $2\,^{\circ}\mathrm{C}$. ΔT_{exp} is thus twice as large as ΔT_{sim}. This difference could be caused by bad thermal conduction between the K_2CO_3 grains and the thermocouple or between the K_2CO_3 grains and the copper surfaces [1]. Both explanations suggest the assumption that 'the model is correct after optimizing for k' could be premature, and the model should be expanded to increase the accuracy of results. It should be noted, however, that one thermocouple was attached directly to the copper wall, leading to the highest possible ΔT. In the simulations, the temperature of the K_2CO_3 a few millimeters away from the wall has been used to calculate ΔT_{sim}, which results in a smaller ΔT and is more representative for the bulk of the sample. While ΔT_{exp} deviates quantitatively from ΔT_{sim}, it is still likely that the model gives a good qualitative analysis of the temperature throughout the sample. Therefore, the placement of the thermocouples is likely to work like intended (i.e. they span the entire sample temperature range) and ΔT_{exp} is a reliable measurement of the maximum temperature difference within the sample.

3.4.3 Conclusion

A copper container was designed with the use of COMSOL Multiphysics to limit ΔT_{sim} to $1\,\mathrm{K}$ so long as the heating/cooling rate does not exceed $\pm 1\,\mathrm{K/min}$. Experiments with the manufactured copper container showed that ΔT_{exp} exceeds this value and reaches up to $2\,\mathrm{K}$. This value should be interpreted as the maximum possible temperature difference within the sample, while the true temperature range within the bulk of the material are smaller. Despite not reaching the goal of $\Delta T_{exp} \leq 1\,\mathrm{K}$, ΔT_{exp} has still been significantly reduced, to allow for measurements with an acceptable uncertainty.

[1] This might matter only because the shape and total contact area of metal with K_2CO_3 is much bigger with the copper container than without it.

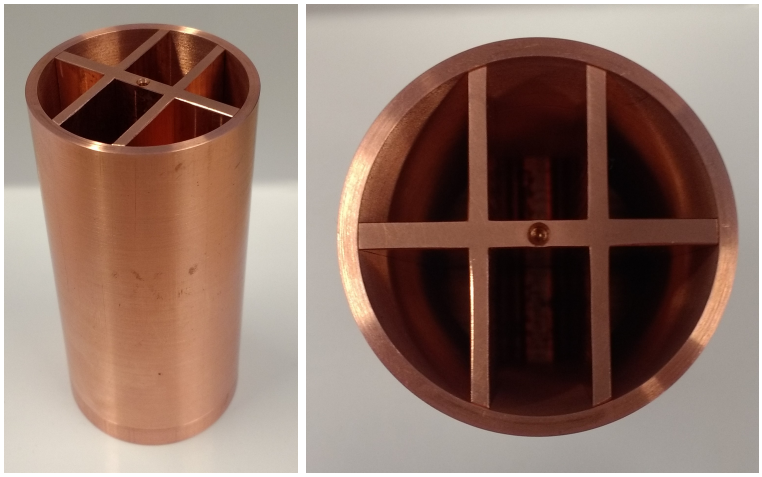

Figure 3.5: The copper container, that can be filled with K_2CO_3 grains and placed inside the sample holder. It is designed with fins to help transport heat from and to the outside walls in order to create a more homogeneous temperature within the sample.

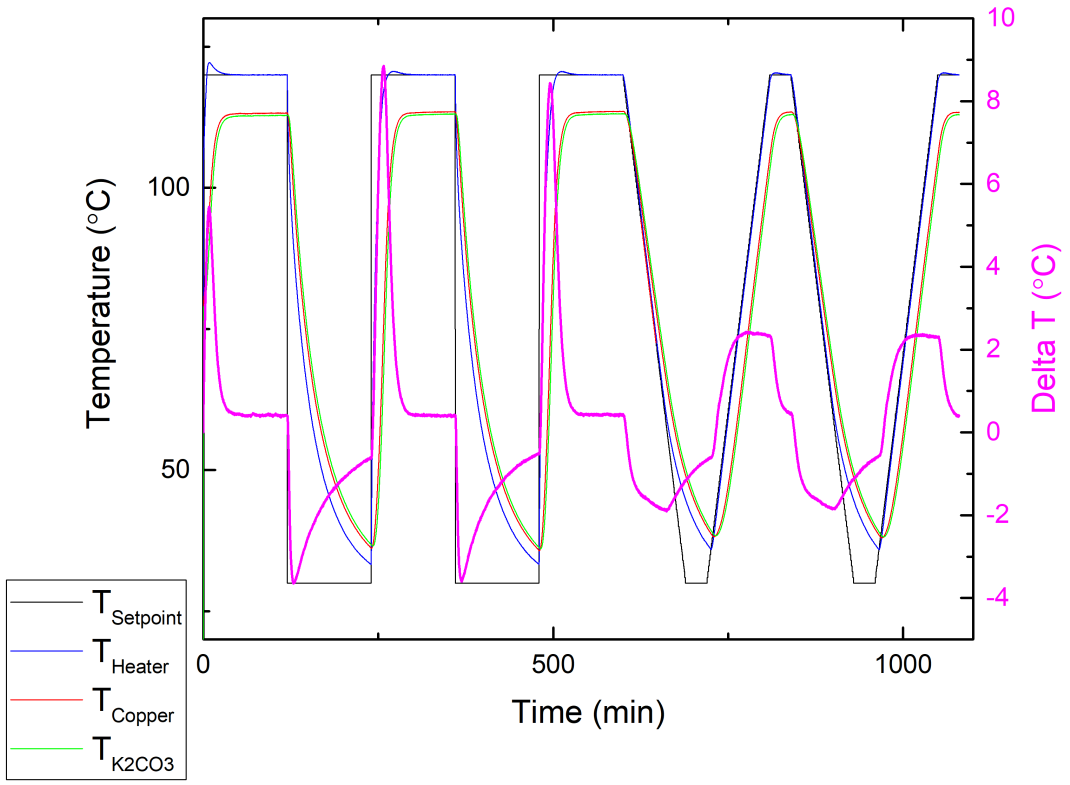

Figure 3.6: The reaction of the system to changes in temperature, without any chemical reactions. The left y-axis shows the temperatures shown in the legend. The right y-axis shows the calculated $\Delta T = \Delta T_{exp} = T_{copper} - T_{K_2CO_3}$. For high heating and cooling rates, ΔT_{exp} reaches up to $+9$ and $-5\,\mathrm{K/min}$ respectively. For rates of $\pm 1\,\mathrm{K/min}$, ΔT_{exp} is limited to about $\pm 2\,\mathrm{K/min}$.

3.5 Sample Preparation

Grains consisting of a K_2CO_3 and graphite composite are sieved to $1.4 - 2.0\,\mathrm{mm}$. The material is stored at room temperature stored in a closed drum to prevent deliquescence. An unwanted possible side reaction of K_2CO_3 is the formation of bicarbonate ($KHCO^3$). To remove any such impurities, the material is fully dehydrated and purified in an oven at $130\,^{\circ}\mathrm{C}$ prior to experiments. Within the setup no CO_2 is present, so no bicarbonate will form.

3.6 Methods

The experiments described in this thesis are divided into roughly two categories:

1. Determining onset temperatures with the goal of defining the boundaries of the metastable zone.
2. Determining induction times with the goal of finding the activation energies of the phase changes.

In this section, both categories of experiments are explained.

3.6.1 Determining Onset Temperatures

To define the boundaries of the metastable zone, the (de)hydration onset temperatures are measured for different water vapor pressures and different heating/cooling rates. To find a hydration onset temperature, a measurement starts with a fully dehydrated sample in equilibrium. The temperature is then gradually lowered isobarically. At some temperature the hydration reactions starts to occur, causing the sample mass to increase and, as the reaction is exothermal, the temperature to rise (or decrease less then before the reaction occurss). The onset temperature is defined as the temperature at which the mass increase and the temperature deviation start to be observable. The sample is hydrated only several percent, as this is enough to determine the onset temperature. The sample is then fully dehydrated again, so the measurement can be repeated.
This measurement is repeated for multiple pressures and different cooling rates. Then, the measurements are also performed starting with a fully hydrated sample, heating the sample to find the dehydration onset temperature. Heating/Cooling rates are chosen in the order of ± 1, ± 0.5, ± 0.1, and $\pm 0.05\,\mathrm{K/min}$.

Data Processing

The experiments are done mostly automated with the help of Matlab, which controls the instruments and stores their measured data. The data file is later loaded into Origin, where it is processed (e.g. noise is filtered, units are converted) and plotted. A part of such a plot can be seen in Figure 3.7, which shows one cycle where a fully dehydrated sample is partially hydrated by lowering the temperature at a fixed rate, and then returned to dehydrated state. Figure 3.7a gives an overview of the cycle including multiple temperatures, the mass, and the pressure. Figure 3.7b shows a zoom-in of the same cycle used for determining the onset temperature. After approximately 154 minutes the mass of the sample starts to increase, indicating the hydration phase change ($K_2CO_3 \rightarrow K_2CO_3{\cdot}1.5H_2O$) is taking place. Also, a bent in the temperature plot can be seen. This is due to the phase change being exothermic, thus slowing down the natural cooling of the setup. To find the onset temperature four linear fit functions are used: on the mass and on $T_{K_2CO_3}$ both before and after the bent. The intersect of the fits (i.e. the time of the bent) is used to determine the moment of onset according to the mass and the temperature. Of these two times the average is taken. At this average onset time, both $T_{K_2CO_3}$ and T_{copper} are evaluated as they approximately span the entire temperature range of the sample[2]. The onset temperature is then the average of these temperatures, with an uncertainty such that both temperature extremes are covered.

[2] In accordance with the previously described COMSOL Multiphysics simulations, the thermocouples are placed such that one is in the coldest location of the sample, and one is in the hottest (by approximation).

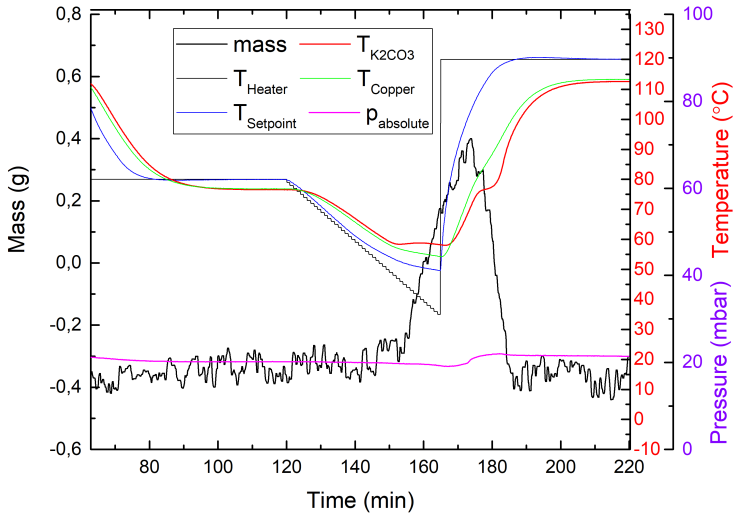

(a)

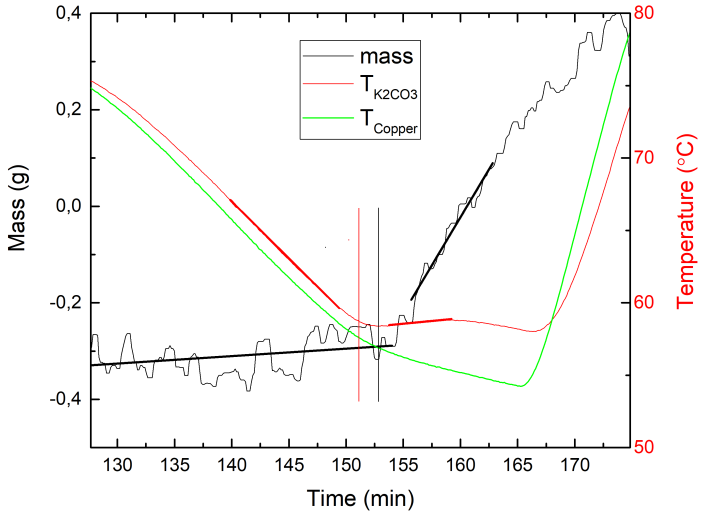

(b)

Figure 3.7: A typical measurement for onset determination. A fully dehydrated sample is partially hydrated by lowering the temperature at a fixed rate, and then returned to dehydrated state. (a) shows an overview of one cycle, and (b) shows the enlarged mass and temperature. There, linear fits are made to the mass and temperature to find the onset temperature. The vertical red and black lines shown the time of intersect of the temperature and mass fits respectively.

This method is manually performed for each single cycle. Each measurement is repeated for multiple cycles, and the average of the different measurements is used. One experiment can contain many cycles (e.g. 10 or 20).

3.6.2 Determining Induction Times

To measure the induction period - the time it takes before (de)hydration occurs in an observable quantity - measurements are done at constant temperature and pressure. For example, to measure a hydration induction time, the ideal experiment is when a completely dehydrated sample in equilibrium is instantly put in a constant atmosphere (p_{H2O}, T) inside the metastable zone, on the hydration side of the phasediagram. Under these conditions, the time until the mass (or temperature) increase due to hydration is observable is measured. This measurement is then repeated for either different temperatures or pressures.
In the setup, it is not possible to instantly change the sample's conditions (p_{H_2O}, T). It is thus not possible to perform the ideal experiment. To approximate the ideal situation whilst partially automating the experiments, a cycle as shown in Figure 3.8 is used. Using notation and steps corresponding to the graph, the different steps are explained below[3]. In this cycle, the electronic valve that connects the water reservoir and the sample is used. Therefore, a distinction is made between $p_{H_2O,reservoir}$ and $p_{H_2O,sample}$. These can differ when the valve is closed. Upon opening the valve, $p_{H_2O,reservoir} = p_{H_2O,sample}$ within seconds.

A. The fully dehydrated sample is in equilibrium at point A. $p_{H_2O,reservoir} = p_{H_2O,sample} = p_A$ and $T_{K_2CO_3} = T_A$. These conditions are maintained for several hours to ensure full dehydration (i.e. the absence of any hydration nuclei).

B. The valve is closed. $T_{K_2CO_3}$ is decreased to $T_B (= T_C)$, whilst T_{H_2O} (governing $p_{H_2O,reservoir}$) is decreased to $T_{H_2O,C}$, thus increasing $p_{H_2O,reservoir}$ to p_C. As the valve remains closed, $p_{H_2O,sample} = p_A = p_B$ is unchanged.

C. When the system is again in equilibrium, the valve is opened. Immediately $p_{H_2O,reservoir}$ drops and $p_{H_2O,sample}$ rises, as the pressure in the system spatially equilibrates. As T_{H_2O} remains near $T_{H_2O,C}$, both $p_{H_2O,reservoir} = p_{H_2O,sample}$ increase relatively quickly to p_C. $T_{K_2CO_3}$ remains equal to $T_B = T_C$.
The system remains at point C for several hours so the induction time at point C can be determined.

A. The system is prepared for another induction time measurement. T_{H_2O} and thus $p_{H_2O,reservoir} = p_{H_2O,sample}$ are decreased to T_A and p_A respectively. $T_{K_2CO_3}$ is increased to T_A. This allows the sample to fully dehydrate, and the cycle to repeat. The cycle is repeated multiple times for each location of C. It can then be repeated for different locations of C (and corresponding A and B).

The data is processed much in the same way as is done for the onset determination. The moment that phase change starts is found by intersecting two linear fits of the mass, as well as intersecting fits for the sample temperature $(T_{K_2CO_3})$ and container temperature (T_{copper}). The induction time is then the time between the opening of the valve and the time corresponding to this intersect.

[3] The actual Matlab script that controls this cycle is slightly more complex. For example, to ensure that the sample is fully dehydrated, a requirement for moving on to the next step is that the mass is (with small deviations allowed) stable for 30 minutes.

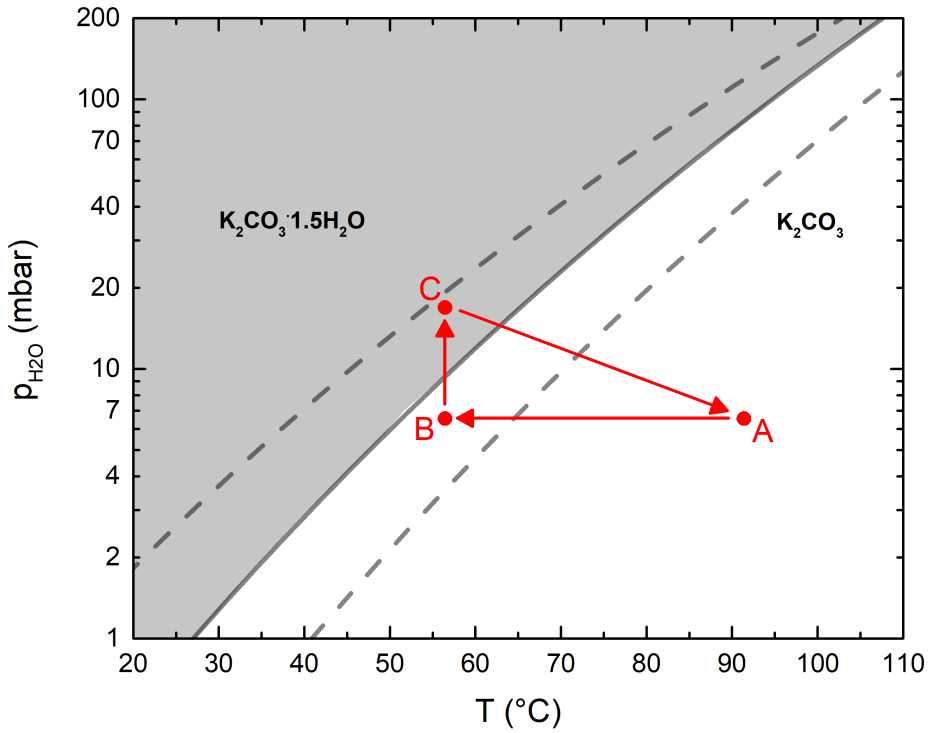

Figure 3.8: A schematic of the cycle used to measure induction times. The sample is dehydrated at point A, and is then brought to point B. The conditions are then quickly changed to point C, where the induction time for p_C, T_C is measured.

3.7 Calibrations

In order to perform the experiments, some of the instruments are calibrated. Other instruments were calibrated in previous research. In this section, calibration of the pressure sensor, the setup's leakage, and the thermocouples is described.

3.7.1 Pressure Sensor

The pressure sensor has been calibrated by using a small closed system with a temperature-controlled water reservoir. This setup consists of the base setup as shown in Figure 3.1 with the electronic valve continuously closed. The system is brought to vacuum by a vacuum pump, so that afterwards $p = p_{H_2O}$. The water reservoir is cycled through different temperatures, and the corresponding pressure responses are measured. The measured pressure, $p_{measured}$, is then compared to the actual pressure p, which is assumed to equal the theoretical water vapor pressure. It is found that $p_{measured}$ deviates from p in two ways:

1. There is an offset, especially for lower pressures ($0-20\,\mathrm{mbar}$), of up to several mbar. Experiments to measure this offset show poor repeatability.

2. After an initial quick reaction of $p_{measured}$ to a change of p, $p_{measured}$ takes several hours to equilibrate. There also seems to be residual sensor hysteresis, although longer measurements are needed to verify this.

It is concluded that $p_{measured}$ is an adequate qualitative measure for the pressure in the setup, whereas for the quantitative value of the pressure the theoretical water vapor pressure should be used (i.e. $p = p_{H_2O}$).

3.7.2 Leakage

All the experiments are performed in near vacuum; without air and with a water vapor pressure of $5 - 200\,\mathrm{mbar}$.
A small amount of air within the setup would not influence the thermodynamics of the phase change reactions, but by forming a non-condensible layer it could block water vapor transport both in the reservoir and in the K_2CO_3 sample[4]. In the reservoir, a non-condensible layer could slow condensation rates of the water vapor, vapor pressure to rise upon dehydration of the K_2CO_3. Such a (sudden) buildup would be measured by the pressure sensor.In the sample, a non-condensible layer could affect hydration kinetics. It is thus desirable to limit any leakage of air into the setup.
A calibration is performed to assess the leakage. Alternating the temperature of the empty sample holder between 30 and $100\,^\circ\mathrm{C}$ over a 68 hour period, the pressure is monitored. Meanwhile, the rest of the setup is kept at a constant $62\,^\circ\mathrm{C}$. The water reservoir temperature is $20\,^\circ\mathrm{C}$, causing a water vapor pressure of $23\,\mathrm{mbar}$.The results of the calibration are shown in Figure 3.9. The measured starting temperature is $20\,\mathrm{mbar}$ – a $3\,\mathrm{mbar}$ offset from the expected $23\,\mathrm{mbar}$. This is attributed to an offset of the pressure sensor. The alternating pressure peaks up and down are caused by the alternation of temperatures. When the temperature changes, the system needs some time to re-equilibrate. Because the peaks hold no information about the leakage, they are masked (marked red in the graph) so they are not used for fitting. A linear fit is made through the data marked by black in the graph and is shown by the red line. The resulting gradient is representative for the rate at which air leaks into the setup, and is $0.021\,\mathrm{mbar/h}$, or $0.51\,\mathrm{mbar/day}$.

3.7.3 Thermocouples

All used thermocouples are calibrated. It is found that upon changing the temperature, the thermocouples respond immediately but take some time (in the order of minutes) to re-equilibrate. The equilibrium measured temperature has a slight offset from the real temperature, which is different for each thermocouple. The conclusion is that the thermocouples can be used with a $1\,\mathrm{K}$ uncertainty at a $3\,\mathrm{K/min}$ heating/cooling rate and $0.5\,\mathrm{K}$ at $\leq 1\,\mathrm{K/min}$.

[4]More precisely, water vapor transport could become diffusion dominated in these regions, as convective forces are negated.

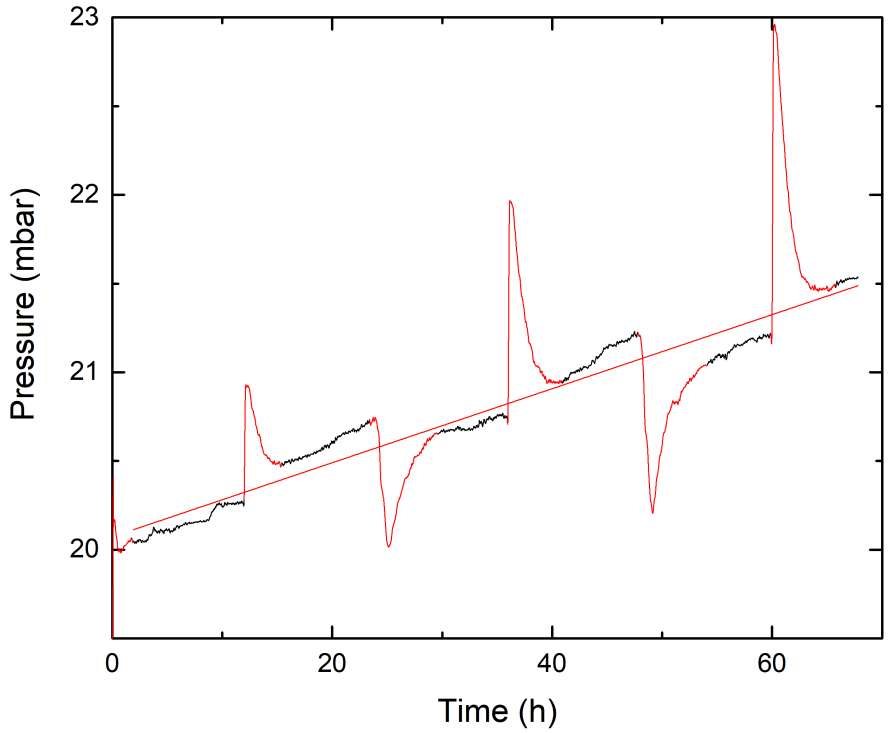

Figure 3.9: Measured pressure as a function of time to asses leakage of the setup. The data marked in black is used for a linear fit, which is shown by the red line.

Chapter 4

Results and Discussion

4.1 Comparison of Experimental Conditions with Sögütoglu's

The results of this thesis will be compared repeatedly with Sögütoglu (2018,2019). To provide a framework for comparison, the experimental conditions from this thesis are compared to those of Sögütoglu. Both this thesis and Sögütoglu's studies measure the gravimetric response of a K_2CO_3 sample to changing temperature and vapor pressure. However, there are multiple differences in the experimental conditions, the most important of which are stated in Table 4.1. The biggest difference is that the current experiments are performed in vacuum – resembling a closed reactor – and Sögötoglu's experiments are performed in atmosphere – resembling an open reactor. This allows for a comparison of thermochemical properties of K_2CO_3 between vacuum and atmosphere. Additional differences are (this thesis compared to Sögütoglu): a much larger sample mass, allowing for more reactor-like conditions; a different material (grains of a K_2CO_3-graphite composite versus pure K_2CO_3 powder), which could influence kinetics and local vapor transport; a higher maximum vapor pressure, which makes this thesis an expansion to Sögütoglu(2019) as well as an atmosphere–vacuum comparison with it. Because these factors could potentially influence kinetics, it is difficult to attribute any different results solely to the vacuum–atmosphere difference. Finally, the current setup is less precise in measuring the mass. Drift, fluctuations, and reactions to pressure and temperature affect the measured mass, as was addressed already in chapter 3. This can make onset and induction observation more difficult.
The experimental methods used for onset temperature and induction time determination in this thesis are very similar to Sögütoglu's. There is a difference in the induction experiments, where for this thesis a cycle approximating the ideal situation is used, as was described in subsection 3.6.2.

Table 4.1: The experimental conditions of this thesis compared to those of Sögütoglu (2019).

	This Thesis	Sögütoglu (2019), TGA
Atmosphere	Vacuum	1 atm
Sample Size	60 g	$\mathcal{O}(10)$ mg
Sample Material	K_2CO_3-graphite composite	Pure K_2CO_3
	Grains	Powder
p_{H2O}	8-200 mbar	0-20 mbar
Mass Measurement Precision	Lower	Higher

4.2 Metastable Zone

The boundaries of the metastable zone have been determined by measuring the onset points for different heating and cooling rates. The resulting phase diagram is presented in Figure 4.1, where the measured onset points are plotted with different symbols for the different heating/cooling rates. For visual ease the error bars are not shown – the temperature uncertainty is 1 to $2\,^{\circ}\mathrm{C}$ for all measurements and the relative pressure uncertainty is $\leq 10\%$. Most onset measurements have been repeated multiple times, and have been averaged to give the shown data points. The data from all four cooling rates are fitted with the Clausius-Clapeyron relation,

$$p = p_0 \cdot \exp\left(\frac{1}{R}\left(\frac{-\Delta H}{T + 273.15} + \Delta S\right)\right), \tag{4.1}$$

with $R = 8.314\,\mathrm{J}\cdot\mathrm{K}^{-1}\cdot\mathrm{mol}^{-1}$ the universal gas constant, $p_0 = 986.92\,\mathrm{mbar}$. The change in enthalpy upon the phase change, ΔH, and the change in entropy, ΔS, are used as fitting parameters. From the dehydration experiments, only the $1\,\mathrm{K/min}$ rate is fitted, because not enough data points are available for other heating rates. For comparison, the dashed gray lines show the metastable zone boundary in atmospheric conditions[6].

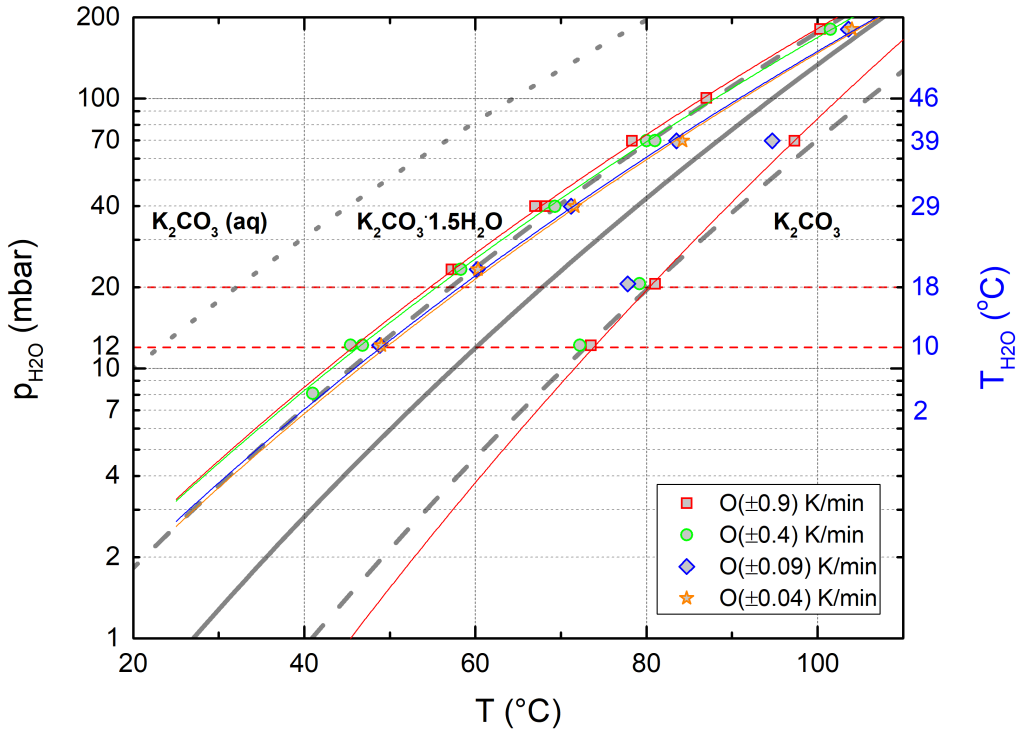

Figure 4.1: The phase diagram of K_2CO_3 including measured onset points for different heating/cooling rates. p_{H_2O} is the water vapor pressure and T_{H_2O} is the corresponding water reservoir temperature. T is the sample temperature. The solid gray line is the phase line, where K_2CO_3 α and β phases are in equilibrium. The dashed gray lines show the metastable boundaries for atmospheric conditions, known from earlier research[6]. The dashed red horizontal lines show the expected working pressures in application conditions. The data for each rate is separately fitted with the Clausius-Clapeyron relation.

The metastable zone boundary corresponds with the Clausius-Clapeyron fits, and thus depends on the heating/cooling rate. At lower rates the material has more time to induce, so the metastable zone boundary is observed closer to the equilibrium phase line. This phenomenon is observed both in vacuum conditions (Figure 4.1) and in atmospheric conditions[6].
One interesting observation for higher temperatures/pressures is that the onset temperatures become more dispersed, so the metastable zone boundary is less well defined. The spread in kinetics, measured by how quickly the sample hydrates [%/min], also increases for higher temperatures. The kinetic data is not presented here, and the phenomenon should be further researched.
Both the Clausius-Clapeyron fits for $\pm 1\,\mathrm{K/min}$ intersect the phase line at $130\,^{\circ}\mathrm{C}$. The $-0.5\,\mathrm{K/min}$ fit intersects at $121\,^{\circ}\mathrm{C}$, and the -0.1 and $-0.05\,\mathrm{K/min}$ both intersect at $110\,^{\circ}\mathrm{C}$. This can be interpreted as the induction time τ becomes smaller for higher (p,T), until eventually reaction starts instantaneously.

4.3 Induction Times and Interfacial Energy

Induction times τ have been determined by putting the sample in a metastable state and measuring the time until a reaction takes place. The measured induction times are plotted against the supersaturation in Figure 4.2a. The experiments are all performed with a sample temperature of $55\,^{\circ}\mathrm{C}$, for different vapor pressures. The induction time is determined in three different ways: the moment of an observable increase in mass, copper temperature, and K_2CO_3 temperature. Each square represents a single measurement. The shown error bars are the reading error. The data is compared to atmospheric experiments of Sögütoglu (2019) in Figure 4.2b.
Logarithmic plots of τ and p/p_{eq} are presented in Figure 4.3, in which Equation 2.12 is fitted to determine the interfacial energy γ. Figure 4.3a en 4.3c show the measured data, including the temperature-determined induction times. Only the mass-determined induction times are used for fitting and, thus, for calculating γ, because the temperature measurements are ambiguous. The mass-determined induction time is compared to Sögütoglu in Figure 4.3b and 4.3d.
Not all measurements have resulted in a data point. For example, immediate induction is sometimes observed for supersaturations that normally show significant induction times. Such a measurement is disregarded. In general, conflicting measurements and filtering out unlikely data can lead to inaccurate results. In particular, known theory and previous results (Sögütoglu) allow for a comparison that can lead to confirmation bias, in which data not matching the expectations is more easily disregarded than data that does match with expectations. For these reasons, it is recommended for future research to perform more induction measurements.

Temperature-determined Induction Times

The temperature-determined induction times (by both T_{copper} and $T_{K_2CO_3}$) do not show a clear trend with changing supersaturation, while the mass-determined induction times do. Therefore, the temperature-determined induction times are not used for fitting. For low supersaturations no temperature change is observed (because reaction ration rates are low and thus heat is released only slowly), so no temperature-determined induction times are shown. For higher supersaturations reaction rates are higher, causing a larger heat release and thus a measurable temperature increase. It can be seen that temperature-determined induction times are generally shorter than mass-determined induction times. This also holds true for individual experiments, where temperature increases are consistently observed earlier than mass increases. This could be caused by differing measurement precision for mass and temperature. A relatively small amount of induction can already give an observable temperature change, while more nucleation sites need to induce before mass increase can be significantly observed. More experiments are required to explain why the temperature-determined induction times do not show a clear trend. Possibly, with more data points a trend similar to mass-determined induction times will emerge.

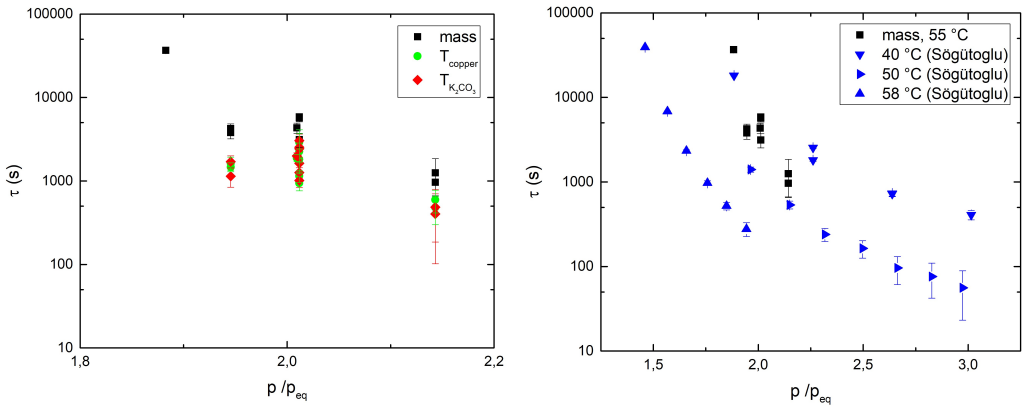

Figure 4.2: The induction time τ as a function the supersaturation p/p_{eq}. The displayed error bars are the reading errors. (a) shows the current results, including the induction times determined measuring the mass, copper temperature, and K_2CO_3 temperature. (b) shows the mass-determined induction time compared to results of Sögütoglu[6]. All the current results are obtained with a sample temperature of $55\,^{\circ}\mathrm{C}$.

Cycling the Material

All induction experiments have been performed with a single sample. While K_2CO_3 is considered a stable material even after many cycles[5], cycling between full dehydration and partial hydration can potentially change local crystal structures and kinetics. In the data there appears to be a trend towards shorter induction times after an increasing number of cycles, although the trend is inconclusive. Further research is suggested to analyze this phenomenon, for example by measuring the induction time for a specific (p,T) point many cycles in a row. The top left data point in Figure 4.2a (bottom right in Figure 4.3a and 4.3c) is possibly unreliable because the corresponding measurement was performed last in time, so the induction time could have been influenced by having used the sample for many cycles. This idea is reinforced by the following observation: in this measurement $\tau = 10\,\mathrm{h}$, whereas an earlier measurement in the same conditions did not find any induction even after $36\,\mathrm{h}$ (no data point plotted).

Nucleation Rate Pre-factor

While the slope of the linear fit equation (Equation 2.12) is most important (as it results in the interfacial energy γ), it is also interesting to evaluate the pre-exponential factor of the nucleation rate, which corresponds to the y-axis intersect in this linear fit. The fits with the current data have a higher y-axis intersect than for Sögütoglu. From Equation 2.12, the intersect corresponds with $\ln(\kappa/c)$, thus an increased intersect means an increased pre-exponential factor

$$\frac{\kappa}{c} = \frac{N_s j \mathcal{Z}}{c}.$$

N_s, the number of nucleation sites, could differ from Sögütoglu because of the different material. j, the rate at which water molecules attach to a nucleus, could differ from Sögütoglu mainly because of the vacuum conditions. c is a kinetic parameter, which could also differ. $\mathcal{Z}$, the Zeldovich factor, should be similar for vacuum and atmospheric conditions. In conclusion, there may be multiple causes for the higher pre-exponential factor, and it is likely a consequence of different kinetics in vacuum and atmosphere.

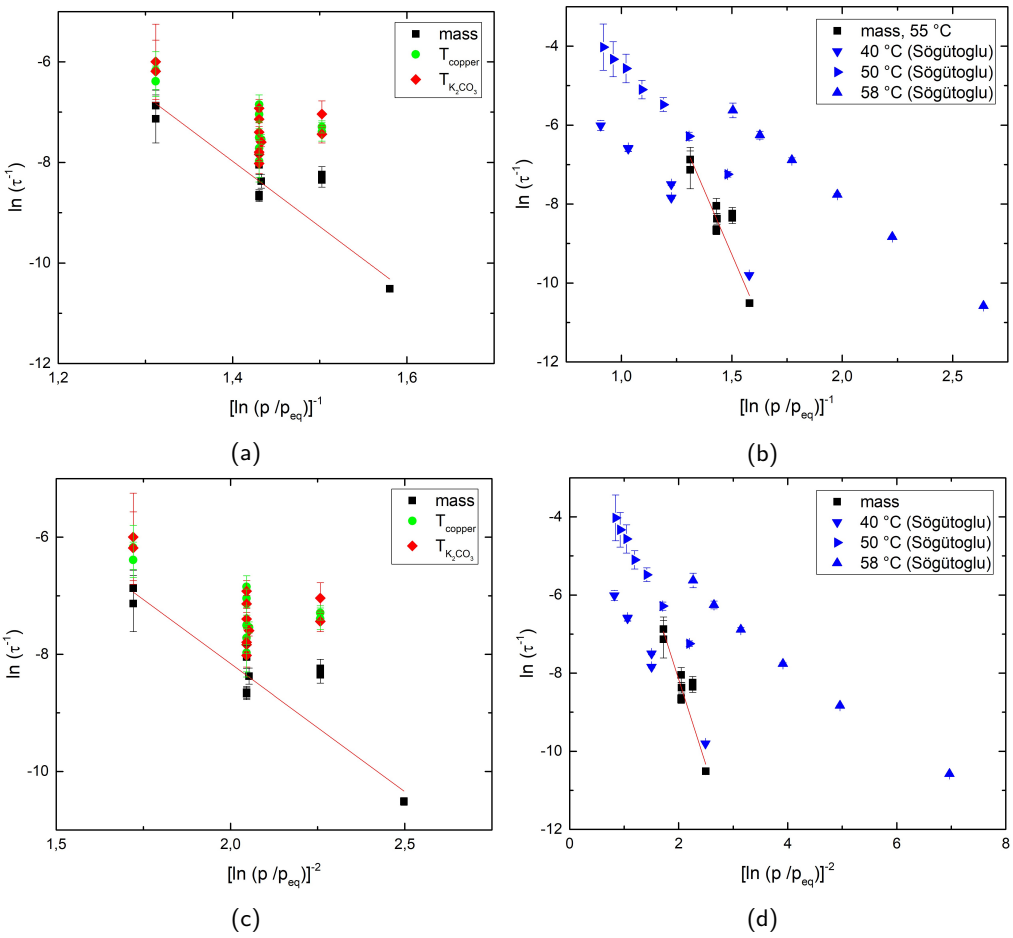

Figure 4.3: The induction time τ as a function of the supersaturation p/p_{eq} logarithmically plotted including a linear fit. The displayed error bars are the reading errors. (a) and (c) show the current results, including the induction times determined measuring the mass, copper temperature, and K_2CO_3 temperature. (b) and (d) show the mass-determined induction time compared to results of Sögütoglu[6]. All the current results are obtained with a sample temperature of $55\,^{\circ}\mathrm{C}$.

Limitations of the Setup

The mass measurement in the currently used setup is less precise than in a professional TGA setup. Right after opening the valve, the pressures and temperatures in the setup shift. The system needs up to ten minutes to re-equilibrate mechanically, in which the mass can drift quite dramatically (i.e. several tenths of grams). As a consequence, short induction times are difficult to measure. Especially using the measured mass, it is impossible to accurately determine an induction time shorter than $1000\,\mathrm{s}$. It might be possible to measure slightly shorter induction times using the measured temperature, although more experiments are required to explore this possibility.

Interfacial Energy

The slope of the fits in Figure 4.3 is used to calculate the surface tension γ, as explained in section 2.2. In Figure 4.2 and 4.3 the shown error bars on τ correspond to the reading errors in individual measurements. However, between different measurements a factor 2 in measured τ is not uncommon, which is a much bigger variation than the reading error. This dispersion is attributed to the stochastic nature of induction. To take this into account a hypothetical scenario is used: instead of the reading

errors, a relative error of 100% on τ is used for fitting Equation 2.12. The resulting γ for 2D disc, 3D hemisphere, and 3D sphere growth patterns are presented in Figure 4.4, where it is also compared to Sögütoglu (2019).
Even with the hypothetically enlarged error bars, the here presented γ for vacuum conditions is still larger than for the atmospheric conditions of Sögütoglu. On the contrary, γ is thermodynamically expected to be independent of surrounding atmosphere. Also, whilst kinetics could well differ between vacuum and atmosphere, kinetics should only affect the pre-exponential factor and not the interfacial energy. The present difference may be caused by experimental differences such as the different material. Most importantly, as the current data set is small, future research should focus on providing more and repeated measurements.

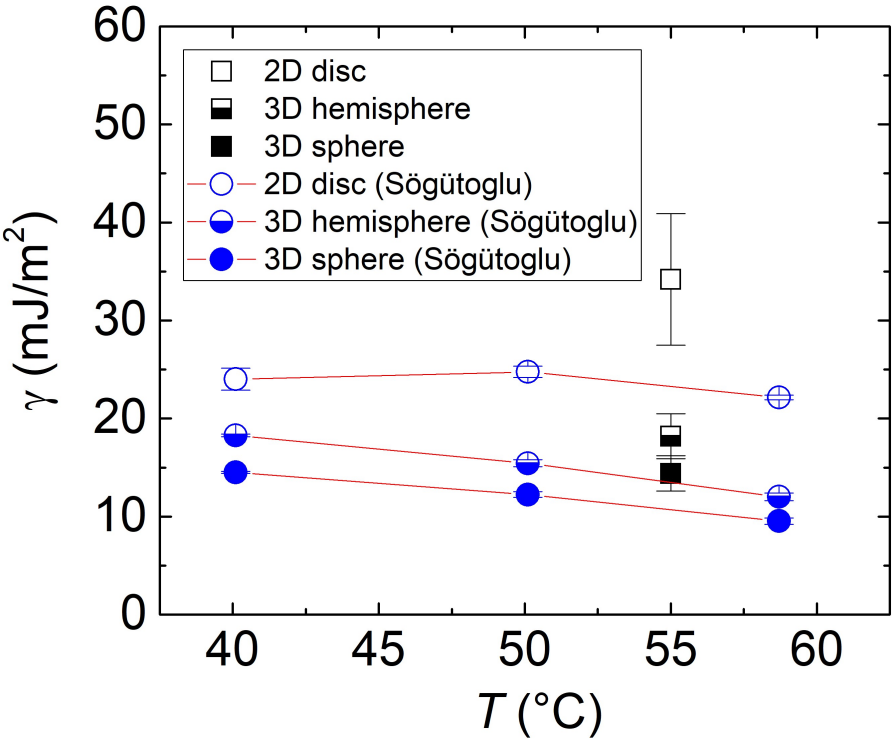

Figure 4.4: Interfacial energies γ of K_2CO_3, calculated from a fit to the induction times with a relative uncertainty of 100%. Current (vacuum) results compared to (atmospheric results of) Sögütoglu (2019).

Nucleation Mechanism

Although the here presented interfacial energy γ is a bit larger than that of Sögütoglu, it is still quite similar to it (especially for the 3D scenarios). This suggests that a comparable hydration mechanism is in place in vacuum as in atmospheric conditions. As Sögütoglu concluded, the hydration of K_2CO_3 seems to take place in a solid-solid transition, mediated through a wetting layer. This mechanism has been elaborated upon in chapter 1. Although the τ measurements show some inconsistencies, performing more experiments will likely only change the calculated γ within the currently presented error bars. It is thus fairly certain that the hydration mechanism is indeed similar for vacuum and atmospheric conditions.
It would be interesting to see how γ progresses for higher (p,T) especially because of the previously observed spread in onset points for higher (p,T). It is possible that a different hydration mechanism is in place for these higher (p,T), so the above conclusions should be considered valid for typical working pressures only. Induction time measurements for high (p,T) are not included in this thesis, and are a recommended focus area for future research.

Sample Size Statistics

Induction is a stochastic process, hence repeating induction measurements will give different τ's and create a statistical distribution. An increase in sample size should suppress variations between measurements, which would give the present $60\,\mathrm{g}$ sample size a unique advantage over the much smaller sample size of conventional TGA. This concept is explored below.
In a simplified view, the underlying statistics of the induction time distribution can be described as follows: each nucleation site s induces after some induction time τ_s. Any macroscopic sample of K_2CO_3 contains $N_s \gg 1$ nucleation sites, where N_s scales with sample size. With the setup it is impossible to detect a single nucleation, so induction is only observed after the induction of some fraction of the nucleation sites which depends on the measurement precision. Because many nucleation sites must induce before an induction time is experimentally measured, the experimental induction time τ_{exp} can be considered to scale with τ_m, the mean of all τ_s:

$$\tau_{exp} \propto f \cdot \tau_m, \tag{4.2}$$

where f is an experimental factor depending on the measurement precision.
Within the metastable zone, the standard deviation for induction at individual nucleation sites S_τ is expected to be very large. Using theory of standard deviation for averages[7], the standard deviation of the measured induction time is

$$S_{\tau_{exp}} \propto S_{\tau_m} = \frac{S_\tau}{\sqrt{N_s}}. \tag{4.3}$$

In short, the standard deviation of the measured induction time $S_{\tau_{exp}}$ should scale with $(\mathrm{sample\ size})^{-1/2}$. This is a simplified model, so it is likely to be not entirely correct. Still, it is clear that the sample used for this thesis, which is much larger than that used by Sögütoglu , should have much less variation between repeated measurements. Hence it is surprising to see a factor 2 in τ between different measurements under identical conditions. Measurements that were performed just after each other do seem to be more correlated than measurements that had more time in between them, although the data set is too small to conclude this with certainty. This suggests that the induction process is very susceptible to changes in experimental conditions that are currently uncontrolled, or that the induction time changes due to cycling.

Chapter 5

Conclusions

This thesis set out to compare the thermochemical behavior of K_2CO_3 in vacuum conditions (resembling a closed reactor) to its behavior in atmosphere (resembling an open reactor) as known from literature. More specifically the goal was to compare the metastable zone (boundaries), induction times and corresponding interfacial energy, and to deduce the hydration mechanism in vacuum. Working towards these goals, some other interesting observations have been made as well. The conclusions are described below.

The metastable zone boundary for application conditions ($\mathcal{O}(10-20)\,\mathrm{mbar}$) is similar for vacuum and atmospheric conditions and is approximately $10\,^{\circ}\mathrm{C}$ wide. For higher (p,T), the metastable zone boundary becomes less well defined, where lower cooling rates give the boundary close to the phase line, and higher rates further away. The fitted and extrapolated metastable zone boundary intersects the phase line at: $130\,^{\circ}\mathrm{C}$ for $\pm 1\,\mathrm{K/min}$, $121\,^{\circ}\mathrm{C}$ for $-0.5\,\mathrm{K/min}$, and $110\,^{\circ}\mathrm{C}$ for both -0.1 and $-0.05\,\mathrm{K/min}$. For fitting to the induction data, there are two fitting parameters: the y-axis intersect, resulting in the nucleation rate pre-factor, and the slope, which is used to calculate the interfacial energy γ. The nucleation rate pre-factor ($\frac{N_s j \mathcal{Z}}{c}$) is higher in vacuum (results from this thesis) than in atmosphere (Sögütoglu). This may have multiple causes, and is likely related to the difference in kinetics between vacuum and atmosphere. The interfacial energy γ found for vacuum conditions is slightly higher than in atmospheric values found by Sögütoglu. Therefore, the hydration mechanism in vacuum for application conditions is likely to be a direct solid-solid transition mediated by a wetting layer, just like Sögütoglu found in atmosphere. Although the induction time data set is small and shows some inconsistencies, it is concluded with fair certainty that the hydration mechanism is indeed similar for vacuum and atmospheric conditions. Other observations of the induction time require more and more methodologically repeated measurements. Some of these, and other interesting observations, are listed below:
-For identical supersaturations, using a sample that has performed more (de)hydration cycles seems to shorten the induction time, although the data set is too small to conclude this with certainty.
-The found temperature-determined induction time is consistently shorter than mass-determined induction time, which can potentially be explained by differing measurement precision for mass and temperature.
-From a statistical point of view, the standard deviation of the measured induction time $S_{\tau_{exp}}$ should scale with $(\mathrm{sample\ size})^{-1/2}$. The variations found in τ for identical supersaturation are larger than would be expected from this theory.
-For identical supersaturations, induction time measurements that were performed just after each other seem to be more correlated than measurements that had more time in between them, although the data set is too small to conclude this with certainty. This suggests that the induction process is very susceptible to changes in experimental conditions that are currently uncontrolled, or that the induction time changes due to cycling.

List of questions to be answered:

- (1) How does the metastable zone for vacuum conditions compare to atmospheric?
- (2) How does the induction time for vacuum conditions compare to atmospheric?
- (3) How does the interfacial energy for vacuum conditions compare to atmospheric?
- (4) How does the reaction mechanism for vacuum conditions compare to atmospheric?

Conclusion: Lijst van bevindingen die relevant zijn voor bovenstaande vragen

- (1) The metastable zone boundary for application conditions ($\mathcal{O}(10-20)\,\mathrm{mbar}$) is similar for vacuum and atmospheric conditions and is approximately $10\,^{\circ}\mathrm{C}$ wide . Verify. Add to resultsDiscussion.
- (1) For higher (p,T), the metastable zone boundary becomes less well defined (or, more spread out), where lower cooling rates give the boundary close to the phase line, and higher rates further away. The kinetics (reaction rate) are also more spread out for higher (p,T)
- (1) The metastable zone boundary (extrapolated) intersects the phase line at: $130\,^{\circ}\mathrm{C}$ for $\pm 1\,\mathrm{K/min}$, $121\,^{\circ}\mathrm{C}$ for $-0.5\,\mathrm{K/min}$, and $110\,^{\circ}\mathrm{C}$ for both -0.1 and $-0.05\,\mathrm{K/min}$.
- (2,0) Temperature-determined induction time is consistently shorter than mass-determined induction time
- (0) Inconclusive: Cycling the material (i.e. ...) shortens the induction time at the same (p,T) conditions.
- (2,0) Nucleation rate pre-factor ($\frac{N_s j Z}{c}$) is higher in vacuum (thesis) than in atmosphere (Sögütoglu). This may have multiple causes.
- (3) γ is slightly higher in vacuum (thesis) than in atmosphere (Sögütoglu).
- (4) The hydration mechanism in vacuum is likely to be a direct solid-solid transition mediated by a wetting layer (just like in atmosphere) for application conditions.
- (0) The standard deviation of the measured induction time $S_{\tau_{exp}}$ should scale with $(\mathrm{sample\ size})^{-1/2}$.
- (0) The variation between experiments is bigger than hence expected. Causes could be: relevant uncontrolled experimental conditions; induction time changes due to cycling.
- (2,0) Induction time measurements that were performed just after each other do seem to be more correlated than measurements that had more time in between them, although the data set is too small to conclude this with certainty.

Chapter 6

Outlook

This thesis set out to compare the thermochemical behavior of K_2CO_3 in vacuum conditions to its behavior in atmosphere. Multiple conclusions have been taken with reasonable certainty, whereas some of the observations are inconclusive and ask for further research. This chapter summarizes the recommendations for future studies.

Expanding the study
This thesis is the result of a Bachelor Final Project and is therefore of limited scope. Many of the results could use more measurements before publishing and for more certain conclusions. In this thesis the metastable zone boundary on the hydration side has been well determined for the expected pressures in an application. Only a few measurements, however, have been performed to the dehydration metastable zone boundary. More onset measurements should be done for dehydration, as well as at higher water vapor pressures, as is described in the next paragraph.

High water vapor pressures
It was shown in the results that the metastable zone boundary becomes less well defined for higher water vapor pressures, while the metastable zone width decreases. It is recommended to do more onset measurements at these high (p,T) conditions and to also measure induction times, with the goal of better understanding the hydration mechanism in these conditions and to determine the process causing the increased spread in metastable zone boundary.

Experimental Conditions
One of the main topics of this thesis is the comparison of current vacuum condition results with earlier atmospheric results. A multitude of experimental differences makes it difficult to take conclusions from the found similarities and differences. Future studies should aim to make a more direct comparison by minimizing the experimental differences. One experimental difference is that this thesis tested K_2CO_3 composite grains in a vacuum setup, whereas Sögütoglu (2018,2019) tested K_2CO_3 powder in atmosphere using TGA. For a more direct comparison, a K_2CO_3 composite grain could be put in a TGA (atmospheric conditions), or K_2CO_3 powder could be put in the current vacuum setup. Both of these alterations would allow for a more direct comparison of the results. One challenge in the latter option might be kinetic limitations due to potentially poor water vapor transport into the bulk powder. Another improvement would be to measure the induction times at $58\,^{\circ}\mathrm{C}$, identical to one ofSögütoglu's experiments, whereas current measurement in this thesis were performed at $55\,^{\circ}\mathrm{C}$.

Cycling
In this thesis the inconclusive observation was made that repeated (de)hydration of a sample decreased its induction times τ for similar (p,T) conditions. This apparent process, from here on referred to as 'cycling', should be studied in a more methodological order as it could be an important phenomenon for understanding TCM's and influence future reactor requirements.
Besides the potential effect of cycling, there are two more variables that could influence the measured

induction time: (1) differences between different samples; (2) currently uncontrolled, but relevant, experimental conditions that might change by exchanging the sample. To measure cycling itself, the induction time of one sample in the same (p,T) conditions should be measured some integer X times in a row. To account for variable (1) (differences between samples), the sample should then be replaced by new samples, which should also be tested X times. To account for variable (2) (change in experimental conditions) a tested sample could be removed from the setup, and then be reinstalled as if it were a new sample. If a change in measured τ is then measured it can be attributed to the experimental changes.

Reaction rates

In this study reaction rates ($\%\ \mathrm{conversion/min}$) have been found to vary between different (p,T) conditions, and depending on pre-nucleation. Understanding the driving forces for reaction rates is highly relevant for future reactors, as a reaction design should strive to achieve a high reaction rate close to the phase line (where, on the contrary, reaction rates are typically low). The results have not been discussed in this thesis, as they were not enough ordered to take conclusions. Experiments designed for studying reaction rates should be performed more methodologically, and a more concrete goal (e.g. is there interest in reaction rate as a function of supersaturation, temperature, or both?) should be designed.

Bibliography

[1] International Energy Agency. Status of Solar Heating/Cooling and Solar Buildings - Country Report - Turkey - http://www.iea-shc.org/country-report-turkey, 2016. 1

[2] P. A.J. Donkers, L. C. Sögütoglu, H. P. Huinink, H. R. Fischer, and O. C.G. Adan. A review of salt hydrates for seasonal heat storage in domestic applications. *Applied Energy*, 199:45–68, 2017. 1

[3] Jelle Houben and P.A.J. Donkers. Thermal conductivity of salt hydrates as TCM. 2017. 14

[4] Vitaly I. Kalikmanov. *Nucleation theory*. 2013. 7, 8

[5] L. C. Sögütoglu, P. A.J. Donkers, H. R. Fischer, H. P. Huinink, and O. C.G. Adan. In-depth investigation of thermochemical performance in a heat battery: Cyclic analysis of K2CO3, MgCl2and Na2S. *Applied Energy*, 215(August 2017):159–173, 2018. 3, 4, 28

[6] Leyla-Cann Sögütoglu, Michael Steiger, Jelle Houben, Daan Biemans, Hartmut R. Fischer, Pim Donkers, Henk Huinink, and Olaf C. G. Adan. Understanding the Hydration Process of Salts: The Impact of a Nucleation Barrier. *Crystal Growth & Design*, (1):acs.cgd.8b01908, 2019. 3, 4, 5, 7, 9, 26, 27, 28, 29

[7] TU/e. *Experimentele Fysica 1*. 2015. 31